COLLEGE OF ENGINEERING

VIRGINIA POLYTECHNIC INSTITUTE AND STATE UNIVERSITY

BLACKSBURG, VIRGINIA

College of Engineering

Virginia Polytechnic Institute and State University

Blacksburg, VA 24061

VPI-E-83-14 April 1983

The Response of Cylindrical Panels Fabricated from Symmetrically and Unsymmetrically Laminated Composite Materials

Douglas M. Carper[1]
Eric R. Johnson[2]
Michael W. Hyer[3]

Department of Engineering Science & Mechanics

Interim Report 32
The NASA-Virginia Tech Composites Program

NASA Cooperative Agreement NCC1-15

Prepared for: Robert G. Thompson, Huey D. Cardon, and Richard L. Boitnott
Impact Dynamics Branch
Structures and Dynamics Division
Structures Directorate
National Aeronautics & Space Administration
Langley Research Center
Hampton, VA 23665

[1]Graduate Student, Engineering Science & Mechanics

[2]Assistant Professor, Aerospace and Ocean Engineering

3Associate Professor, Engineering Science & Mechanics

BIBLIOGRAPHIC DATA SHEET	1. Report No. VPI-E-83-14	2.	3. Recipient's Accession No.

4. Title and Subtitle

THE RESPONSE OF CYLINDRICAL PANELS FABRICATED FROM SYMMETRICALLY AND UNSYMMETRICALLY LAMINATED COMPOSITE MATERIALS

5. Report Date April 1983

6.

7. Author(s)

D. M. Carper, E. R. Johnson, M. W. Hyer

8. Performing Organization Rept. No. VPI-E-83-14

9. Performing Organization Name and Address

Virginia Polytechnic Institute & State University
Engineering Science & Mechanics
Blacksburg, Virginia 24061

10. Project/Task/Work Unit No.

11. Contract/Grant No. CA NCC1-15

12. Sponsoring Organization Name and Address

National Aeronautics & Space Administration
Langley Research Center
Hampton, Virginia 23665

13. Type of Report & Period Covered

14.

15. Supplementary Notes

16. Abstracts

Equations are developed which govern the deflection response of long cylindrical panels subjected to a line load. The line load is directed toward the center of curvature of the panel, is located at an arbitrary point along the arc length of the panel, and is inclined at an arbitrary angle relative to the radial direction. Only the geometrically linear problem is considered and the spatial dependence in the problem is reduced to one independent variable, specifically, the arc length along the panel. The problem is thus solvable in closed form. Both symmetrically laminated and the less common unsymmetrically laminated simply supported panels are studied. The unsymmetrically laminated case was considered because the natural shape of an unsymmetric laminate is cylindrical. Results are presented which show the influence of the location and inclination of the line load on panel deflection. Shallow and deep panels are considered. Both the symmetric and unsymmetric panels exhibit similar behavior, the unsymmetric configurations being less stiff. Limited experimental results are presented.

17. Key Words and Document Analysis. 17a. Descriptors

fiber-reinforced composite laminates, composite shells, unsymmetric composite laminates

17b. Identifiers/Open-Ended Terms

17c. COSATI Field/Group 24-01 39-02 39-07 39-08 39-01

18. Availability Statement	19. Security Class (This Report)	21. No. of Pages
DISTRIBUTION UNLIMITED	UNCLASSIFIED	74
	20. Security Class (This	22. Price

TABLE OF CONTENTS

LIST OF FIGURES

1. INTRODUCTION

The vast majority of composite laminates in use today are fabricated so that the material properties are symmetric with respect to the laminate's geometric midsurface. To have symmetric material properties a laminate must be fabricated so that for every lamina above the geometric midsurface with specific material properties, thickness, and fiber orientation, there is a lamina below the midsurface with identical material properties, thickness, and fiber orientation. A laminate so constructed will not exhibit bending-stretching coupling in its elastic response to external loads. Coping with analyses which must include bending-stretching coupling effects can be difficult. Thus to simplify the analysis of composites, laminates are fabricated with midsurface symmetry of material properties. However, to make a laminate symmetric only to simplify the analysis is a penalty on the performance of the composite. In practice, symmetry is generally achieved by adding a sufficient number of layers to the laminate. From a strength or stiffness measure, these lamina may not be necessary. However, adding the lamina most certainly increases the weight of a structure. It may be that unsymmetric laminates are actually desirable. Experimental evidence has shown that unsymmetrically laminated composites, which are flat at their elevated cure temperature often cure to a shape closely approximated by a right circular cylinder. The out-of-plane warping of the cured laminate is a direct result of bending-stretching coupling. However, the cylindrical characteristic is contrary to the predictions of classical lamination theory [1,2]. The classical theory predicts the

cured shape of all unsymmetrically laminated composites to be saddle-like, having their principle curvatures of opposite sign but not necessarily of the same magnitude. For some unsymmetric laminates, however, the saddle-shape does appear. It was felt by many investigators that the observed cylindrical shapes were due to problems with curing, moisture absorption, or other unwanted effects in the fabrication process. However, a systematic experimental study [3] has shown that the phenomena is repeatable and whether a cured unsymmetric laminate assumes a cylindrical shape or a saddle shape depends on the thickness of the laminate compared with a characteristic in-plane length. Thin laminates cure into the shape of a right circular cylinder while thicker laminates conform, at least qualitatively, to the saddle-shape predictions of the classical theory. This characteristic of thin unsymmetric laminates is felt to be very important because of the large number of components on aircraft which are cylindrical in nature. In addition, fabrication of these cylindrical shapes is not much more difficult than the fabrication of flat laminates. No expensive mandrels or forms are needed; the laminate simply cools to the cylindrical shape.

Recently a theory has been developed which accounts for this behavior of unsymmetric laminates [4]. The theory is a nonlinear extension of classical lamination theory and at present is limited to the analysis of laminates having their lamina oriented at either 0° or 90° relative to some global coordinate system. However, the predictions of the theory agree well with the limited amount of experimental data available. The theory indicates that the radius of curvature of the cylinder is a function of the lamina orientations (i.e. $[90_4/0_4]_T$, $[90_5/0_3]_T$,

etc.) and the thermo-elastic properties (E_1, E_2, α_1, α_2, ...) of the individual lamina. The theory is being extended to account for arbitrary lamina orientations. It appears, even at this early stage of the development of the theory, that this phenomena should be strongly considered as a way to fabricate cylindrical components from composite materials. The next question is: How useful are these cylinders? Do they buckle easily? Do they have unusual vibration characteristics? How do they respond to point loads, pressure loads, etc.? Perhaps any unusual response characteristics can be off-set by the ease of fabrication considerations. To answer the just-mentioned questions, a rational step-by-step series of analyses of unsymmetrically laminated cylinders is in order. These analyses should range from linear analyses to nonlinear analyses, static and dynamic, steady-state dynamic and transient dynamic, prebuckling and postbuckling. The analyses should procede in such a way that potential problems are first examined at a simple level, say, with linear analyses, and then if no problems appear, cylinders should be examined at a more complicated level, say, with nonlinear analyses. At all times the behavior of the unsymmetric laminates should be compared with a symmetric counterpart, its competitor based on current thinking. This paper reports on the first step in examining the utility of cylinders fabricated from unsymmetric lay-ups. The paper examines the static structural response of an unsymmetrically laminated long cylindrical panel subject to a line load acting inward. A line load, though simple, is felt to represent one of the more severe types of static loadings a laminate can encounter. The analysis presented is a geometrically linear and elastically linear analysis.

The report begins in the next section by describing the geometry and the nomenclature of the cylindrical panel. The section continues by describing the kinematics of the assumed deformation. From the kinematics such fundamental quantities as strain, cross-section rotation, and curvature are established. Next, the nomenclature associated with the applied load is discussed and the internal force resultants are defined. Newton's second law is applied to a small section of the panel to establish static equilibrium equations in terms of the internal force resultants and the applied load. Since the panels studied have only 0° and 90° lamina, the constitutive behavior of the cylindrical panel is represented by an orthotropic stress-strain relation. The out-of-plane stresses are assumed to be negligible and so the constitutive behavior ultimately reduces to the familiar A, B, and D matrices. In the study of these unsymmetrically laminated cylindrical panels it is shown to be convenient to define a reference surface other than the laminate's geometric mid-plane. The location of the reference surface through-the-thickness is related to the material properties of the panel. This aspect is discussed in detail. After the discussion of the constitutive behavior, the boundary conditions and transitions conditions at the point load are examined. This next section concludes by establishing the differential equations which govern the deformation behavior of the panel.

The third section of this report is devoted to solving the governing equations. The boundary and transitions conditions are applied and closed-formed expressions for the deformation of the panel, as a function of spatial position along the panel, are obtained. The fourth section

of the paper presents numerical results regarding deflections, stiffnesses, and strains of several representative panels. The numerical results for unsymmetrically laminated panels are examined in the context of results for a symmetrically laminated panel which use the same amount of material. This type of comparison is done to illustrate any advantages or disadvantages of unsymmetrically laminated panels. The formulation and results presented herein are valid for arbitrarily deep cylindrical panels. A formulation and numerical results are presented for shallow panels. Comparisons between the deep theory and the shallow theory are made. The main purpose of this comparison is to establish whether deepness of cylindrical composite panels is a purely geometric property, as it is for metal panels, or whether it involves material properties as well. This latter idea has been suggested by some investigators.

Finally, the fifth section reports on some experimental results. The force deflection characteristics of a $[90_4/0_4]_T$ and a $[(0/90)_2]_s$ T300/5208 graphite-epoxy cylindrical panel are compared with theoretical predictions. The purpose of this comparison is to determine if predicted differences between symmetric and unsymmetric panels are observable. The experimental set-up is briefly described as is the correlation between the theory and experiment.

2. PROBLEM DEFINITION

Geometry

Figure 1 illustrates the basic notation associated with the cylinder geometry. The undeformed circular cylinder has a center of curvature at O and has a semi-opening angle θ_o. The laminate has thickness h. There are two surfaces within the laminate to be considered. Normally, analyses of laminated plates and shells deal with the geometric midsurface of the laminates. All geometry, boundary conditions, and other information is referenced to this surface. To date, analyses of composite panels have dealt primarily with symmetric laminates. In these cases it is natural to consider the geometric midsurface as the reference surface from which to describe the panel's geometry and deformation. As will be shown later, due to the elastic bending-stretching coupling inherent in unsymmetric laminates, it advantageous to consider another surface as the reference surface. Thus the analysis here will discuss both the geometric midsurface and the reference surface. These two different surfaces are illustrated in Fig. 1. The laminate midsurface and reference surface are a distance 'd' apart. The quantity d, to be defined later, is a material property. The radius of curvature of the laminate midsurface is 'a' while the radius of curvature of the reference surface is 'R.' These quantitites are related by

$$R = a + d. \tag{1}$$

The arch rise, denoted as 'H,' is measured at midspan and is the vertical distance from the midsurface to the horizontal line joining the end-points of the midsurface arc. The variable θ is the independent

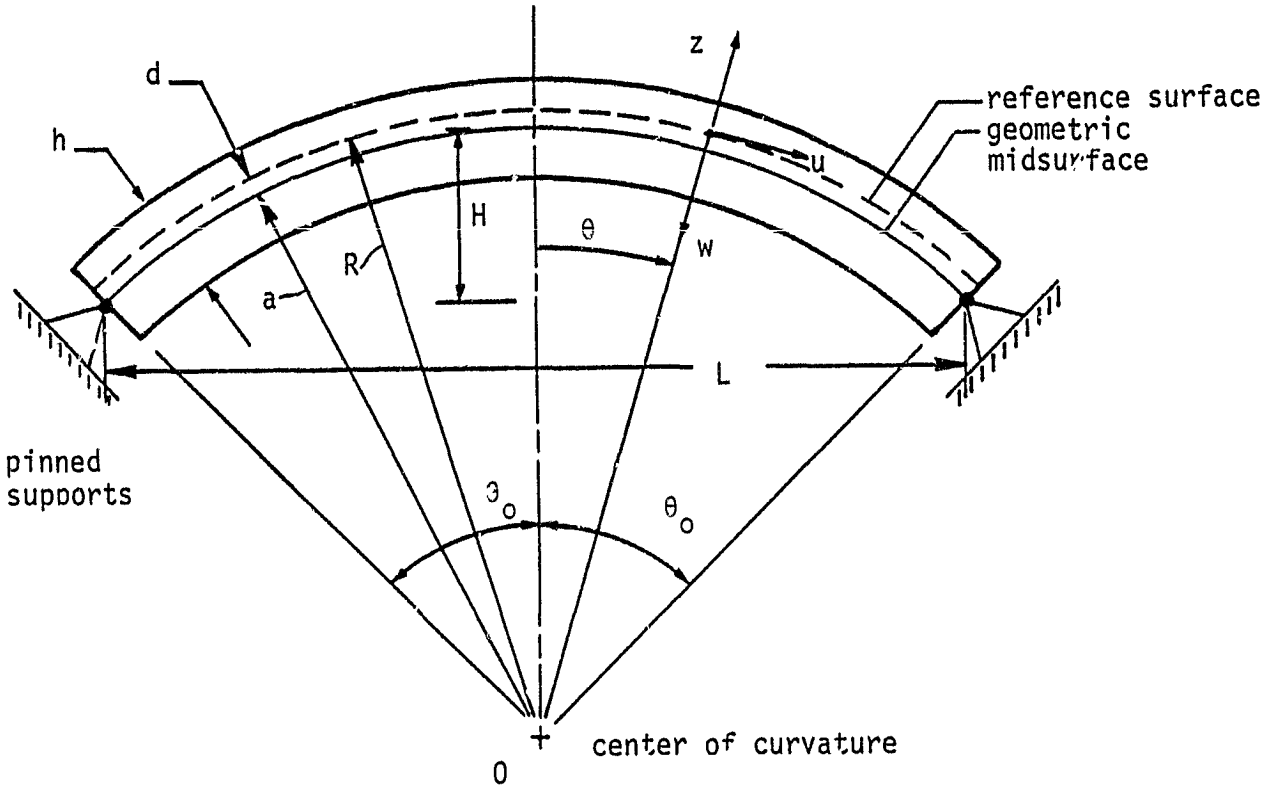

Fig. 1 Cylinder Geometry

spatial variable. It describes the angular position along the arch, and it is measured positive clockwise from the midspan vertical. Position through the thickness of the laminate is denoted as 'z,' with z = 0 at the laminate reference surface.

The radial displacement of the reference surface is denoted as 'w,' positive w being towards the center of curvature. The circumferential displacement of the reference surface is denoted as 'u,' with positive u being to the right. In this analysis, $w = w(\theta)$ and $u = u(\theta)$.

Illustrated in Fig. 1 are pinned supports, the pins acting at the ends of the geometric midsurface. The supports are constrained to remain a fixed horizontal distance apart, this distance being denoted as 'L.' The results presented here are restricted to these pinned conditions but sufficient information is given in deriving the governing equations to allow other support conditions, e.g., clamped, to be studied.

Assumed Deformation of the Reference Surface

Figure 2 depicts the kinematics of the assumed deformation. Due to the applied load, each point on the panel displaces an amount $\overline{\Delta}$ and the cross-section at each point rotates through an angle Ω. In the notation used here, the overbar denotes a vector quantity. The unit vectors $\hat{i}_r$ and $\hat{i}_\theta$ denote unit vectors normal to and tangent to the undeformed reference surface. Likewise, the unit vectors $\hat{n}$ and $\hat{t}$ denote unit vectors normal to and tangent to the deformed reference surface. The orientation of these vectors are all a function of position along the panel. The location of a point on the undeformed reference surface is given by

$$\overline{R} = R\hat{i}_r \, . \qquad (2)$$

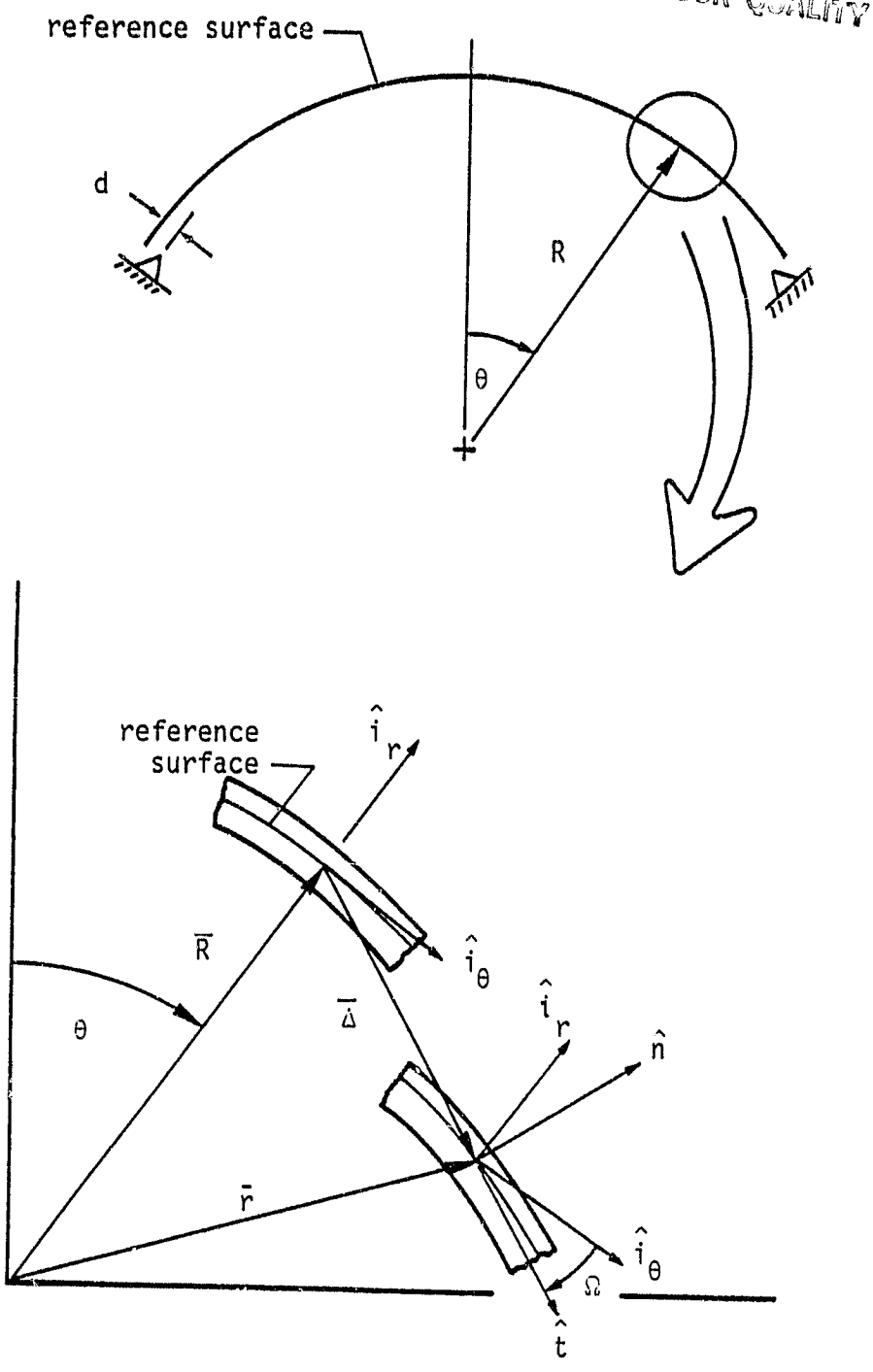

Fig. 2 Kinematics of Reference Surface Deformations

The location of that point after deformation is located by

$$\bar{r} = \bar{R} + \bar{\Delta} \ . \tag{3}$$

The displacement of the point is represented by

$$\bar{\Delta} = -w(\theta)\hat{i}_r + u(\theta)\hat{i}_\theta \ . \tag{4}$$

Using Eqs. 2-4, the extensional deformation of the reference surface can be determined. If dS represents the magnitude of an element of arc length of the undeformed reference surface and ds represents the magnitude of the arc length of that element when it is deformed, then by definition the extensional strain of the reference surface is

$$\varepsilon_\theta = \frac{ds - dS}{dS} \ . \tag{5}$$

Arc length in the undeformed geometry is

$$d\bar{R} = \frac{d}{d\theta}\left(R\hat{i}_r(\theta)\right)d\theta = R\hat{i}_\theta(\theta)d\theta, \tag{6}$$

where use is made of the fact that

$$\frac{d\hat{i}_r(\theta)}{d\theta} = \hat{i}_\theta(\theta) \ . \tag{7}$$

The magnitude of the arc length in the undeformed geometry is

$$dS = \sqrt{d\bar{R}\cdot d\bar{R}} = Rd\theta \ . \tag{8}$$

In the deformed geometry arc length is defined similarly, namely,

$$d\bar{r} = \left[\frac{d\bar{R}}{d\theta} + \frac{d\bar{\Delta}}{d\theta}\right] d\theta \tag{9}$$

$$= \left[R\hat{i}_\theta(\theta) + \frac{d}{d\theta}\left(-w(\theta)\hat{i}_r(\theta) + u(\theta)\hat{i}_\theta(\theta)\right)\right] d\theta. \tag{10}$$

Using Eq. 8, the notation $(\,)' = \frac{d}{d\theta}$, and the relation

$$\frac{d\hat{i}_\theta(\theta)}{d\theta} = -\hat{i}_r(\theta) \ , \tag{11}$$

Eq. 10 becomes

$$d\bar{r} = R\hat{i}_\theta - w'\hat{i}_r - w\hat{i}_\theta + u'\hat{i}_\theta - u\hat{i}_r \, d\theta \tag{12}$$

$$= \left[-\left(\frac{w' + u}{R}\right)\hat{i}_r + \left(1 + \frac{u' - w}{R}\right)\hat{i}_\theta\right] Rd\theta \ . \tag{13}$$

By defining

$$\Gamma_r = -\left(\frac{w' + u}{R}\right) \text{and } \Gamma_\theta = \left(\frac{u' - w}{R}\right) \ , \tag{14),(15}$$

the deformed arc length can be written as

$$d\bar{r} = \left[(1 + \Gamma_\theta)\hat{i}_\theta + \Gamma_r\hat{i}_r\right]dS \ . \tag{16}$$

The magnitude of the deformed arc length now becomes

$$ds = \sqrt{d\bar{r}\cdot d\bar{r}} = \left[(1 + \Gamma_\theta)^2 + \Gamma_r^2\right]^{1/2} dS \ . \tag{17}$$

The extensional strain of a line element is then computed directly to be

$$\varepsilon_\theta = \frac{ds - dS}{dS} = \sqrt{(1 + \Gamma_\theta)^2 + \Gamma_r^2} - 1 \ . \tag{18}$$

Rewriting this as

$$\varepsilon_\theta = \sqrt{1 + 2\Gamma_\theta + \Gamma_\theta^2 + \Gamma_r^2} - 1, \tag{19}$$

and using the binomial expansion of the first term, the extensional strain can be written as

$$\varepsilon_\theta = \Gamma_\theta + \frac{1}{2}\Gamma_r^2 + O(\Gamma^3) . \tag{20}$$

Assuming the deformations of the panel are small,

$$0 < |\Gamma_\theta| << 1 \qquad \text{and} \qquad 0 < |\Gamma_r| << 1 , \tag{21),(22}$$

the higher order terms can be dropped. The strain-displacement relationship then becomes linear, namely,

$$\varepsilon_\theta = \Gamma_\theta = \frac{u' - w}{R} . \tag{23}$$

The rotation, Ω, and the curvature, κ, at points of the reference surface can be related to u and w by further analysis of the kinematics. Again referring to Fig. 2, the tangent and normal to the deformed reference surface are related by the rotation to the tangent and normal of the undeformed surface. These relations are

$$\hat{t} = - \sin(\Omega)\hat{i}_r + \cos(\Omega)\hat{i}_\theta \tag{24}$$

$$\hat{n} = \cos(\Omega)\hat{i}_r + \sin(\Omega)\hat{i}_\theta . \tag{25}$$

By definition

$$\hat{t} \equiv \frac{d\bar{r}}{ds} . \tag{26}$$

Using previous results,

$$\hat{t} \equiv \frac{d\bar{r}}{ds} = \frac{1}{1 + \varepsilon_\theta} \frac{d\bar{r}}{dS} = \left[(1 + \Gamma_\theta)\hat{i}_\theta + \Gamma_r \hat{i}_r \right] \frac{1}{1 + \varepsilon_\theta} . \tag{27}$$

Comparing Eq. 24 and Eq. 27,

$$\cos(\Omega) = \frac{1 + \Gamma_\theta}{1 + \varepsilon_\theta} , \qquad \sin(\Omega) = \frac{-\Gamma_r}{1 + \varepsilon_\theta} . \tag{28),(29}$$

Thus the tangent of the rotation is given by

$$\tan(\Omega) = \frac{-\Gamma_r}{1 + \Gamma_\theta} . \tag{30}$$

If the deformations are small, then in addition to Eqs. 21 and 22 being true,

$$1 + \varepsilon_\theta \simeq 1 . \tag{31}$$

For these conditions the rotations are approximated by

$$\Omega \simeq -\Gamma_r = \frac{w' + u}{R} . \tag{32}$$

The curvature of the reference surface is defined by

$$\frac{d\hat{t}}{ds} \equiv -\kappa \hat{n} \qquad \text{and} \qquad \frac{d\hat{n}}{ds} \equiv -\kappa \hat{t} . \tag{33),(34}$$

Again, using previous results, Eq. 33 can be expanded as

$$\frac{d\hat{t}}{ds} = \frac{d\hat{t}}{dS}\frac{dS}{ds} = \frac{1}{1+\varepsilon_\theta}\frac{d\hat{t}}{dS} = \frac{1}{R(1+\varepsilon_\theta)}\frac{d\hat{t}}{d\theta} . \tag{35}$$

Using Eq. 24 in Eq. 35 leads to

$$\frac{d\hat{t}}{ds} = \frac{1}{R(1+\varepsilon_\theta)} \left\{ - \cos(\Omega)\,\Omega'\hat{i}_r - \sin(\Omega)\,\hat{i}_\theta - \sin(\Omega)\,\Omega'\hat{i}_\theta - \cos(\Omega)\,\hat{i}_r \right\} . \tag{36}$$

Regrouping results in

$$\frac{d\hat{t}}{ds} = \frac{1+\Omega'}{R(1+\varepsilon_\theta)} \left\{ - \cos(\Omega)\hat{i}_r - \sin(\Omega)\hat{i}_\theta \right\} . \tag{37}$$

Substituting Eq. 25 in Eq. 37 leads directly to an equation of the form of Eq. 33, namely

$$\frac{d\hat{t}}{ds} = - \frac{(1+\Omega')}{R(1+\varepsilon_\theta)}\hat{n} . \tag{38}$$

Therefore, curvature is defined to be

$$\kappa = \frac{1+\Omega'}{R(1+\varepsilon_\theta)} . \tag{39}$$

For small deformations

$$\kappa = \frac{1}{R} + \frac{\Omega'}{R} = \kappa_o + \frac{\Omega'}{R} , \tag{40}$$

κ_o being the initial curvature of the reference surface. Substituting for the definition of Ω, Eq. 32, the curvature can be related to u and w by

$$\kappa = \kappa_o + \frac{w'' + u'}{R^2} . \qquad (41)$$

Deformations off the Reference Surface

A similiar kinematic analysis can be developed for lines parallel to the reference surface. Figure 3 shows the deformation of a point which is a distance z away from the reference surface. For purposes of illustration, the thickness of the laminate has been exaggerated in Fig. 3. Due to the applied load, the point displaces by an amount $\bar{\Delta}_z$. The subscript z is used to denote off-reference-surface position. It is assumed that deformations normal to the reference surface, i.e. through-the-thickness deformations, are negligible in this analysis and that there are no transverse shearing deformations. Thus, in the deformed state, the point is still a distance z from the reference surface and the distance z is measured along the normal to the deformed reference surface.

The extensional strain on a parallel line is also determined by examining arc lengths. The undeformed location of the point off the reference surface is

$$\bar{R}_z = (R + z)\,\hat{i}_r . \qquad (42)$$

From this,

$$d\bar{R}_z = (R + z)d\theta\hat{i}_\theta = \left(1 + \frac{z}{R}\right) dS\hat{i}_\theta . \qquad (43)$$

and

$$dS_z = \sqrt{d\bar{R}_z \cdot d\bar{R}_z} = (1 + z\kappa_o)dS . \qquad (44)$$

In the deformed geometry, the point is located by

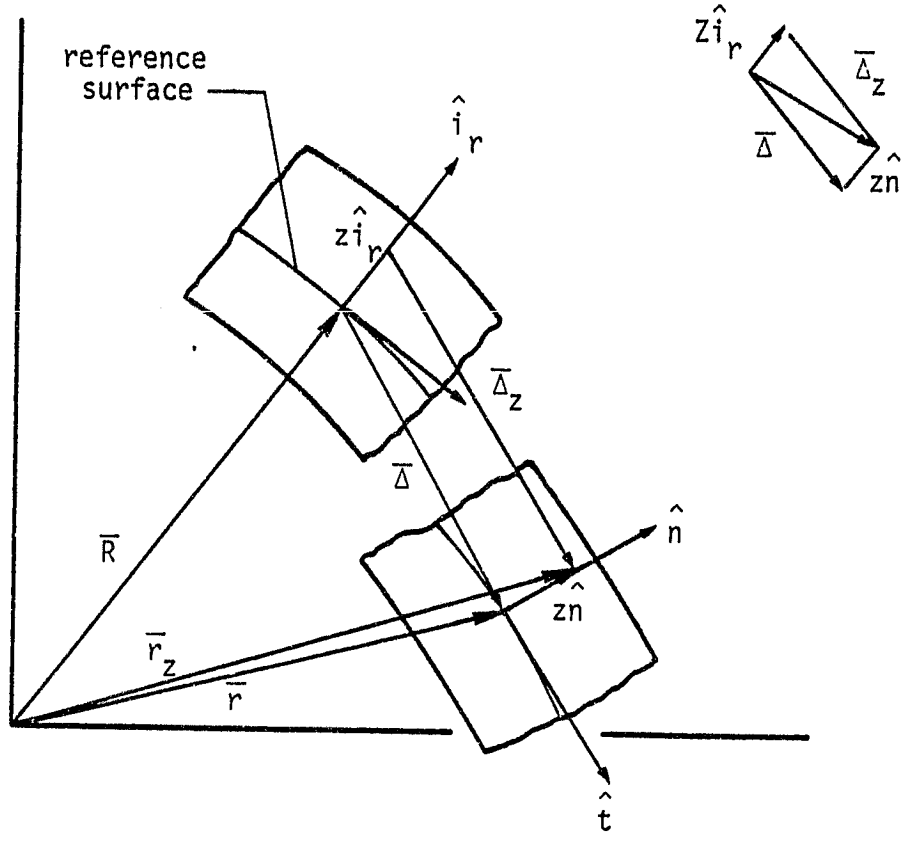

Fig. 3 Kinematics of Deformation Off the Reference Surface

$$\bar{r}_z = \bar{r} + z\hat{n} \ . \tag{45}$$

The deformed arc length can be determined by

$$d\bar{r}_z = \left(\frac{d\bar{r}}{ds} + z \frac{d\hat{n}}{ds} \right) ds = (1 + z\kappa)\, \hat{t}\, ds \tag{46}$$

$$d\bar{r}_z = (1 + \varepsilon_\theta)(1 + z\kappa)\, \hat{t}\, dS. \tag{47}$$

In going from Eq. 46 to Eq. 47, Eqs. (26), (34) and (5) were used. The magnitude of the deformed arc length is

$$ds_z = \sqrt{d\bar{r} \cdot d\bar{r}} = (1 + \varepsilon_\theta)(1 + z\kappa)dS \ . \tag{48}$$

Substituting Eqs. 44 and 48 into the definition of extensional strain,

$$E_\theta = \frac{ds_z - dS_z}{dS_z} \ , \tag{49}$$

leads directly to

$$E_\theta = (1 + \varepsilon_\theta)(1 + z\kappa)(1 + z\kappa_o)^{-1} - 1 \ . \tag{50}$$

Expanding the first two terms and using the binomial expansion of the third terms results in

$$E_\theta = \varepsilon_\theta + z(1 + \varepsilon_\theta)(\kappa - \kappa_o) + O(z^2) \ . \tag{51}$$

For small deformations, the extensional strains on parallel surfaces become, using Eq. 31,

$$E_\theta = \varepsilon_\theta + z(\kappa - \kappa_o) \ . \tag{52}$$

Parallel surface displacements can be computed in terms of reference surface displacements and rotations by considering the geometry of Fig. 3. From the figure

$$z\hat{i}_r + \bar{\Delta}_z = \bar{\Delta} + z\hat{n} \ . \tag{53}$$

Using Eqs. 4 and 25 and grouping terms produces

$$\bar{\Delta}_z = [-w + z(\cos(\Omega) - 1)]\hat{i}_r + [u + z \sin(\Omega)]\hat{i}_\theta \ . \tag{54}$$

If $\bar{\Delta}_z$ is written as

$$\bar{\Delta}_z = -w(\theta,z)\hat{i}_r + u(\theta,z)\hat{i}\theta \ , \tag{55}$$

then by association in Eqs. 54 and 55,

$$w(\theta,z) = w(\theta) + z(1 - \cos(\Omega(\theta))) \tag{56}$$

$$u(\theta,z) = u(\theta) + z \sin(\Omega(\theta)) \ . \tag{57}$$

For small rotations, $\cos(\Omega) \simeq 1$,

$$w(\theta,z) = w(\theta) \ , \tag{58}$$

and

$$u(\theta,z) = u(\theta) + z\Omega(\theta) \ . \tag{59}$$

Applied Loads, Internal Force Resultants, and Static Equilibrium Equations

The load analyzed in this study is a line load of intensity P, with P in units of force per unit length along the generator direction.

Referring to Fig. 4, the force P is positive when directed toward the center of curvature and the load acts at some arbitrary location on the span denoted by $\theta = \psi$. The load is inclined from the radial direction by an angle α.

The internal force resultants are illustrated in Fig. 4. The in-plane (membrane) force, N, is assumed positive in tension. The positive sense of the shear resultant, V, and moment resultant, M, are indicated in the figure. These resultants are assumed to act at the reference surface and, as in a shell theory, are defined per unit length along the generator or x-direction.

To determine the governing equilibrium equations, a small portion of laminate is isolated. The pertinent forces acting in this portion of the laminate are illustrated in Fig. 5. Since this is a linear theory, the forces are illustrated in and Newton's Law will be applied in the undeformed geometry. Even though the interest here is in a line load, a distributed load $q(\theta)$ is shown in the figure for generality. It is assumed spatially uniform in the x-coordinate and has units of force per unit reference surface area.

Referring to Fig. 5 and summing forces in the normal, $\hat{i}_r$, direction leads to

$$\frac{dV}{d\theta} - N = Rq \cos(\alpha) \ . \tag{60}$$

Summing forces in the tangential, $\hat{i}_\theta$, direction results in

$$\frac{dN}{d\theta} + V = Rq \sin(\alpha) \ . \tag{61}$$

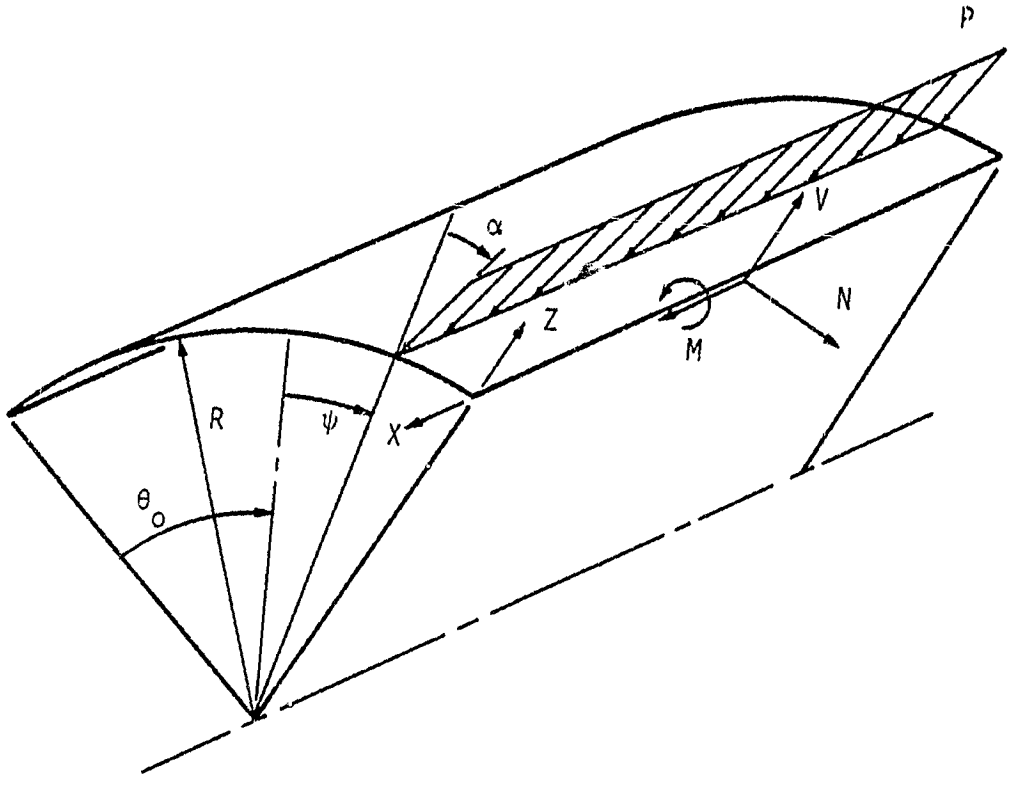

Fig. 4 Applied Forces and Internal Force Resultants

Finally, moment equilibrium of the element requires

$$\frac{dM}{d\theta} + RV = 0 \ . \tag{62}$$

Equations 60 - 62 are the static equilibrium equations which govern the behavior of the cylinder under load.

Constitutive Behavior and the Determination of the Reference Surface Location

The constitutive equations for a lamina are

$$\sigma_x = \overline{Q}_{11}E_x + \overline{Q}_{12}E_\theta \tag{63}$$

$$\sigma_\theta = \overline{Q}_{12}E_x + \overline{Q}_{22}E_\theta \tag{64}$$

$$\tau_{x\theta} = \overline{Q}_{66}\gamma_{x\theta} \ , \tag{65}$$

where E_x, E_θ, $\gamma_{x\theta}$ are the strains and σ_x, σ_θ, $\tau_{x\theta}$ are the stresses. Because the laminates in this study are made from lamina with fibers either in the 0° or 90° direction relative to the x-direction, $\overline{Q}_{i6} = 0$, $i = 1,2$.

For a panel which is long in the x-direction, it is assumed that

$$E_x = \gamma_{x\theta} = 0 \ , \tag{66}$$

such that

$$\sigma_x = \overline{Q}_{12}E_\theta \ , \tag{67}$$

$$\sigma_\theta = \overline{Q}_{22}E_\theta \ , \tag{68}$$

$$\tau_{xy} = 0 \ . \tag{69}$$

For a beam it is assumed that the transverse stresses are zero, i.e. $\sigma_x = 0$ in this case. Hence

$$\sigma_\theta = \bar{Q}_{22} \left(1 - \frac{\bar{Q}_{12}^2}{\bar{Q}_{11}\bar{Q}_{22}}\right) E_\theta \ . \tag{70}$$

In either formulation the constitutive equation can be written as

$$\sigma_\theta = Q^*_{22} E_\theta \ , \tag{71}$$

where

$$Q^*_{22} = \begin{cases} \bar{Q}_{22} \text{ for a long panel} \\ \bar{Q}_{22} \left(1 - \dfrac{\bar{Q}_{12}^2}{\bar{Q}_{11}\bar{Q}_{22}}\right) \text{ for a beam.} \end{cases}$$

It appears the factor $\bar{Q}_{12}^2/\bar{Q}_{11}\bar{Q}_{22}$ is small with respect to 1 for the practical case. For example, consider a 0° ply of graphite-epoxy. From Jones [1, pp. 46-51],

$$\bar{Q}_{11} = Q_{11} = \frac{E_1}{1 - \nu_{12}\nu_{21}} \tag{72}$$

$$\bar{Q}_{22} = Q_{22} = \frac{E_2}{1 - \nu_{12}\nu_{21}} \tag{73}$$

$$\bar{Q}_{12} = Q_{12} = \frac{\nu_{12}E_2}{1 - \nu_{12}\nu_{21}} \tag{74}$$

Thus

$$\frac{\bar{Q}_{12}^2}{\bar{Q}_{11}\bar{Q}_{22}} = \frac{\nu_{12}^2 E_2}{E_1} = \frac{(0.21)^2 1.7 \text{ msi}}{20 \text{ msi}} = 0.0037485 \tag{75}$$

which is, in fact, small with respect to unity. Therefore $Q_{22}^* = \bar{Q}_{22}$ is exact for a long panel and is a good approximation for a beam or arch.

The definitions of the stress resultants for the reference surface are

$$N = \int_{-(\frac{h}{2}+d)}^{\frac{h}{2}-d} \sigma_\theta \, dz \qquad M = -\int_{-(\frac{h}{2}+d)}^{\frac{h}{2}-d} z\sigma_\theta \, dz \tag{76),(77}$$

Using the constitive relation, Eq. 71, the definition of parallel surface strain, Eq. 52, and integrating, Eqs. 76 and 77 become

$$N = A_{22}\varepsilon_\theta + B_{22}(\kappa - \kappa_o) \tag{78}$$

$$M = -B_{22}\varepsilon_\theta - D_{22}(\kappa - \kappa_o) \tag{79}$$

where

$$(A_{22}, B_{22}, D_{22}) = \int_{-(\frac{h}{2}+d)}^{\frac{h}{2}-d} Q_{22}^*(1, z, z^2) \, dz \tag{80}$$

For the middle surface, making the change of variable $z = \bar{z} - d$ and substituting into Eq. 80 yields

$$A_{22} = \bar{A}_{22} \tag{81}$$

$$B_{22} = \bar{B}_{22} - d\bar{A}_{22} \tag{82}$$

$$D_{22} = \bar{D}_{22} - 2d\,\bar{B}_{22} + d^2\bar{A}_{22}, \tag{83}$$

in which

$$(\bar{A}_{22}, \bar{B}_{22}, \bar{D}_{22}) = \int_{-\frac{h}{2}}^{\frac{h}{2}} Q^*_{22}\,(1, \bar{z}, \bar{z}^2)\,d\bar{z} \tag{84}$$

are the stiffnesses for the middle surface. To uncouple the constitutive equations requires

$$B_{22} = 0 = \bar{B}_{22} - d\bar{A}_{22}, \tag{85}$$

so

$$d = \frac{\bar{B}_{22}}{\bar{A}_{22}} \tag{86}$$

and

$$D_{22} = \bar{D}_{22} - \frac{\bar{B}_{22}^2}{\bar{A}_{22}}\,. \tag{87}$$

The barred stiffnesses are the stiffnesses typically associated with classical lamination theory [1, pp. 154-155]. Using the uncoupled reference surface, Eqs. 78 and 79 reduce to

$$N = A_{22}\epsilon_\theta \qquad \text{and} \qquad M = -D_{22}(\kappa - \kappa_0) \qquad (88),(89)$$

Boundary Conditions

Care must be exercised in the application of the boundary conditions. All boundary conditions must be stipulated in the context of the laminate reference surface, as opposed to the laminate midsurface.

For pinned supports at the middle surface, there is no radial or tangential displacement, that is,

$$w(\pm\theta_0,-d) = 0 \qquad (90)$$

$$u(\pm\theta_0,-d) = 0 \qquad (91)$$

In terms of the reference surface displacement, these conditions are, using Eqs. 58 and 59,

$$w(\pm\theta_0,-d) = w(\pm\theta_0) = 0 \qquad (92)$$

$$u(\pm\theta_0,-d) = u(\pm\theta_0) - d\Omega(\pm\theta_0) = 0 \qquad (93)$$

Using the definition of Ω, Eq. 32, and defining

$$\frac{d}{R} = \delta \ , \qquad (94)$$

the boundary condition for zero tangential displacement at the middle surface becomes

$$(1 - \delta)u(\pm\theta_0) - \delta w'(\pm\theta_0) = 0 \ . \qquad (95)$$

At the pinned supports the bending moment for the middle surface vanishes. If $\overline{V}$, $\overline{N}$, and $\overline{M}$ are the force variables for the middle surfaces and V, N, and M are the corresponding force variables for the reference surface, the following static equivalence holds.

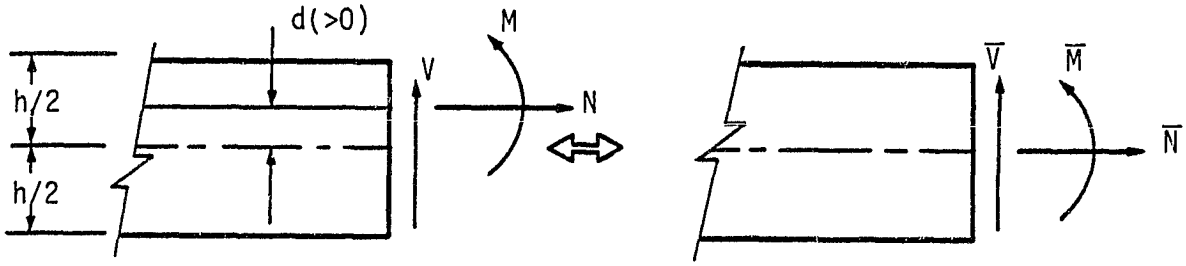

$$V = \overline{V} \qquad \overline{V} = V \tag{96a}$$

$$N = \overline{N} \qquad \overline{N} = N \tag{96b}$$

$$M = \overline{M} + d\overline{N} \qquad \overline{M} = M - dN \tag{96c}$$

The moment-free boundary condition, at the middle surface, is then

$$\overline{M}\,(\pm\theta_o) = 0\ . \tag{97}$$

Referred to the reference surface this condition becomes

$$M(\pm\theta_o) - dN(\pm\theta_o) = 0\ . \tag{98}$$

Using the constitutive relations, Eqs. 88 and 89, Eq. 98 becomes

$$- D_{22}(\kappa(\pm\vartheta_0) - \kappa_0) - dA_{22}\varepsilon_\vartheta\ (\pm\vartheta_0) = 0\ . \tag{99}$$

Using the definition of κ and ε_ϑ, Eqs. 23 and 41, and defining

$$\lambda = \frac{dRA_{22}}{D_{22}}\ , \tag{100}$$

the moment-free boundary condition can be written as

$$w''(\pm\vartheta_0) + (1 + \lambda)u'(\pm\vartheta_0) + w(\pm\vartheta_0) = 0\ . \tag{101}$$

By virtue of the vanishing radial displacements at the supports, Eq. 92, Eq. 101 simplifies to

$$w''(\pm\vartheta_0) + (1 + \lambda)u'(\pm\vartheta_0) = 0. \tag{102}$$

Equations 90, 95, and 102 become the pinned end boundary conditions on the kinematic variables $u(\vartheta)$ and $w(\vartheta)$.

Transition Conditions at the Point Load

Consider the distributed force per unit reference surface area $q(\vartheta)$ to degenerate to a line load per unit generator direction located at $\vartheta = \psi$ as shown in Fig. 5. Define

$$Rq(\vartheta) = P\delta(\vartheta - \psi)\ , \tag{103}$$

where δ in this equation is the Dirac delta function. The equilibrium equations, Eqs. 60-62, become

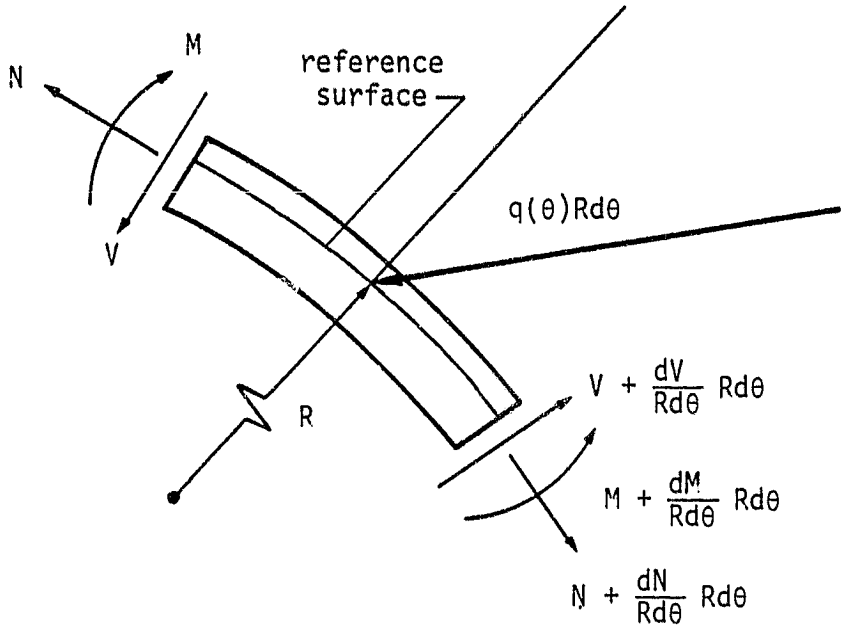

Fig. 5 Equilibrium of a Small Element of Laminate

$$\frac{dV}{d\theta} - N = P\delta(\theta - \psi) \cos \alpha \tag{104}$$

$$\frac{dN}{d\theta} + V = P\delta(\theta - \psi) \sin \alpha \tag{105}$$

$$\frac{dM}{d\theta} + RV = 0 \ . \tag{106}$$

Integrating these equations between $\psi - \varepsilon$ and $\psi + \varepsilon$, $\varepsilon > 0$, results in

$$\int_{\psi - \varepsilon}^{\psi + \varepsilon} \frac{dV}{d\theta} \, d\theta - \int_{\psi - \varepsilon}^{\psi + \varepsilon} N \, d\theta = P \cos \alpha \int_{\psi - \varepsilon}^{\psi + \varepsilon} \delta(\theta - \psi) \, d\theta \tag{107}$$

$$\int_{\psi - \varepsilon}^{\psi + \varepsilon} \frac{dN}{d\theta} \, d\theta + \int_{\psi - \varepsilon}^{\psi + \varepsilon} V \, d\theta = P \sin \alpha \int_{\psi - \varepsilon}^{\psi + \varepsilon} \delta(\theta - \psi) \, d\theta \tag{108}$$

$$\int_{\psi - \varepsilon}^{\psi + \varepsilon} \frac{dM}{d\theta} \, d\theta + \int_{\psi - \varepsilon}^{\psi + \varepsilon} RV \, d\theta = 0 \ . \tag{109}$$

The limit of these equations as $\varepsilon \to 0$ becomes

$$V(\psi^+) - V(\psi^-) = P \cos \alpha \tag{110}$$

$$N(\psi^+) - N(\psi^-) = P \sin \alpha \tag{111}$$

$$M(\psi^+) - M(\psi^-) = 0 \ . \tag{112}$$

These same relations can be obtained by considering a free-body diagram of a panel segment at the location of the line load. From these relations it is clear that the shear and tangential force resultants, V and N,

experience a jump at the location of the line load. The moment, however, is continuous. The continuity condition on M is similiar to the continuity condition on several kinematic quantities which remain continuous at the line load. The kinematic quantities which remain continuous are the tangential displacement, the radial displacement, and the cross-sectional rotation. Specifically,

$$w(\psi^+) = w(\psi^-) \tag{113}$$

$$u(\psi^+) = u(\psi^-) \tag{114}$$

$$\Omega(\psi^+) = \Omega(\psi^-) \ . \tag{115}$$

All transition conditions can be stipulated in terms of the fundamental kinematic variables $u(\theta)$ and $w(\theta)$ by substitution of previously defined quantitites. Working first with those quantities which are continucus at the point load, continuity of rotation, Eq. 115, becomes

$$\frac{w'(\psi^+) + u(\psi^+)}{R} = \frac{w'(\psi^-) + u(\psi^-)}{R} \ . \tag{116}$$

Equation 32 was used for this equality. By virtue of the continuity of the tangential displacements, Eq. 114, continuity of rotations becomes

$$w'(\psi^+) = w'(\psi^-) \ . \tag{117}$$

The jump in the membrane force, Eq. 111, can be represented with the aid of Eq. 88 as

$$A_{22}(\varepsilon_\theta(\psi^+) - \varepsilon_\theta(\psi^-)) = P \sin \alpha \ . \tag{118}$$

From the definiton of ε_θ, Eq. 23, this equation becomes, with a slight rearrangement of terms and using continuity of radial displacements, Eq. 113,

$$u'(\psi^-) + \frac{PR \sin \alpha}{A_{22}} = u'(\psi^+) \ . \tag{119}$$

By using the constitutive relation between moment and curvature, Eq. 89, continuity of moment, Eq. 112, becomes

$$-D_{22}(\kappa(\psi^+) - \kappa_o) = -D_{22}(\kappa(\psi^-) - \kappa_o) \ . \tag{120}$$

From the definition of κ, Eq. 41, continuity of moment reduces to,

$$w''(\psi^+) + u'(\psi^+) = w''(\psi^-) + u'(\psi^-) \ . \tag{121}$$

Finally, the jump in the shear force can be examined. Since shear deformations are ignored the shear force must be written in terms of the other force variables by using the equilibrium equations. Using Eq. 62, the jump in the shear force, Eq. 110, can be stated as

$$-\frac{1}{R} M'(\psi^+) + \frac{1}{R} M'(\psi^-) = P \cos \alpha \ . \tag{122}$$

Using steps similiar to the previous steps, this condition can be written in terms of kinematic quantities as

$$w'''(\psi^-) + u''(\psi^-) + \frac{PR^3 \cos \alpha}{D_{22}} = w'''(\psi^+) + u''(\psi^+) \ . \tag{123}$$

Equations 113, 114, 117, 119, 121, and 123 are the conditons the kinematic variables $u(\theta)$ and $w(\theta)$ must satisfy at the point of application of the load.

Summary of Equations

For convenience the important equations are summarized here. The equations, as a whole, constitute a properly formulated boundary value problem which can be used to study the linear elastic response of an arbitrarily deep cylindrical laminated composite panel to a line load. A symmetrically laminated panel is but a special case.

The equilibrium equations in the intervals $-\theta_o<\theta<\psi$ and $\psi<\theta<\theta_o$ are:

$$V' - N = 0 \qquad (q = 0 \text{ for line load}) \tag{60}$$

$$N' + V = 0 \qquad (q = 0 \text{ for line load}) \tag{61}$$

$$M' + RV = 0 \, . \tag{62}$$

The constitutive behavior of the panels is:

$$N = A_{22}\varepsilon_\theta = A_{22}\left(\frac{u' - w}{R}\right) \tag{88),(23}$$

$$M = -D_{22}(\kappa - \kappa_o) = -D_{22}\left(\frac{w'' + u'}{R^2}\right) . \tag{89),(41}$$

The boundary conditions for the pinned supports are:

$$\text{radial disp.} = 0: \qquad w(\pm\theta_o) = 0 \tag{92}$$

$$\text{tangential disp} = 0: \quad (1 - \delta)u(\pm\theta_o) - \delta w'(\pm\theta_o) = 0 \tag{95}$$

$$\text{moment} = 0: \qquad w''(\pm\theta_o) + (1 + \lambda)u'(\pm\theta_o) = 0 \tag{102}$$

At the line load the following transition conditions must be enforced:

continuity of radial disp.: $$w(\psi^-) = w(\psi^+) \tag{113}$$

continuity of tangential disp.: $$u(\psi^-) = u(\psi^+) \tag{114}$$

continuity of rotations: $$w'(\psi^-) = w'(\psi^+) \tag{117}$$

jump in membrane force: $$u'(\psi^-) + \frac{PR \sin \alpha}{A_{22}} = u'(\psi^+) \tag{119}$$

continuity of moment: $$w''(\psi^-) + u'(\psi^-) = w''(\psi^+) + u'(\psi^+) \tag{121}$$

jump in shear force:

$$w'''(\psi^-) + u''(\psi^-) + \frac{PR^3 \cos \alpha}{D_{22}} = w'''(\psi^+) + u''(\psi^+) \tag{123}$$

By virtue of the nature of the problem, there will be two solutions to the homogeneous governing equations given by Eqs. 60-62. One solution will represent the radial and tangential displacements of that portion of the panel to the left of the point load. The other solution will represent the displacements of the panel to the right of the point load. These two solutions will be related through the transition conditions and each solution will satisfy the boundary conditions pertinent to that portion of the panel.

3. SOLUTION TO GOVERNING EQUATIONS

General Solution to the Differential Equations

From Eq. 61 with q = 0

$$V = -N' \ . \tag{124}$$

Substituting this into Eqs. 60 and 62 yields

$$N'' + N = 0 \tag{125}$$

$$M' - RN' = 0 \tag{126}$$

By Eqs. 88 and 89 the equations become

$$\varepsilon_\theta'' + \varepsilon_\theta = 0 \tag{127}$$

and

$$D_{22}(\kappa - \kappa_o)' + RA_{22}\varepsilon_\theta' = 0 \tag{128}$$

The solution to Eq. 127 is

$$\varepsilon_\theta = A_1 \cos\theta + A_2 \sin\theta \ . \tag{129}$$

Integration of Eq. 128 produces

$$D_{22}(\kappa - \kappa_o) + RA_{22}\varepsilon_\theta = A_3 R \ . \tag{130}$$

Using the definition of the reference surface strain, ε_θ, and curvature, κ, Eqs. 23 and 41, Eqs. 129 and 130 become

$$u' = w + RA_1 \cos\theta + RA_2 \sin\theta \tag{131}$$

$$w'' + u' = -\frac{R^3 A_{22}}{D_{22}}\left(A_1 \cos\theta + A_2 \sin\theta\right) + \frac{R^3}{D_{22}} A_3 \, . \tag{132}$$

Subtracting the two equations and defining

$$\phi_1 = \frac{R^3}{D_{22}} \tag{133}$$

$$\phi_2 = R + \frac{R^3 A_{22}}{D_{22}} \tag{134}$$

results in an equation for $w(\theta)$, namely

$$w'' + w = -A_1\phi_2 \cos\theta - A_2\phi_2 \sin\theta + \phi_1 A_3 \tag{135}$$

The solution to this equation is

$$w(\theta) = -A_1 \frac{\phi_2}{2}\, \theta \sin\theta + A_2 \frac{\phi_2}{2}\, \theta \cos\theta + A_3\phi_1 + A_4 \cos\theta + A_5 \sin\theta \, . \tag{136}$$

Substituting into Eq. 131 and integrating once leads to the expression for $u(\theta)$, specifically,

$$u(\theta) = A_1\left[\left(R - \frac{\phi_2}{2}\right)\sin\theta + \frac{\phi_2}{2}\,\theta\cos\theta\right] + A_2\left[-\left(R - \frac{\phi_2}{2}\right)\cos\theta + \frac{\phi_2}{2}\,\theta\sin\theta\right] + A_3\phi_1\theta + A_4 \sin\theta - A_5 \cos\theta + A_6 \, . \tag{137}$$

Note, Eqs. 136 and 137 are valid in regions of the panel both to the left and to the right of the point of application of the line load. However, constants A_1 through A_6 will be different for each region. In what follows the superscript of +'s or -'s will be used to denote whether the various quantitites being discussed pertain to regions of the panel to the right or to the left, respectively, of the line load. Thus the solution for $w(\theta)$ and $u(\theta)$ to the left of the point load will involve constants A_1^- through A_6^- while the solution for $w(\theta)$ and $u(\theta)$ to the right of the point load will involve constants A_1^+ through A_6^+.

Application of the Boundary and Transition Conditions

Since the boundary conditions and transition conditions have been written in terms of the kinematic quantities $u(\theta)$ and $w(\theta)$, application of these conditions to find the twelve unknown constants A_1^+ through A_6^+ and A_1^- through A_6^- is straight-forward. In terms of the twelve constants, the conditions lead to the following twelve equations:

radial displacement at $\theta = -\theta_o$ is zero:

$$\phi_1 A_3^- - \left\{ A_5^- + \frac{\phi_2 \theta_o}{2} A_1^- \right\} \sin \theta_o + \left\{ A_4^- - \frac{\phi_2 \theta_o}{2} A_2^- \right\} \cos \theta_o = 0 \tag{138}$$

radial displacement at $\theta = +\theta_o$ is zero:

$$\phi_1 A_3^+ + \left\{ A_5^+ - \frac{\phi_2 \theta_o}{2} A_1^+ \right\} \sin \theta_o + \left\{ A_4^+ + \frac{\phi_2 \theta_o}{2} A_2^+ \right\} \cos \theta_o = 0 \tag{139}$$

tangential displacement at $\vartheta = -\vartheta_o$ is zero:

$$(1 - \delta)\left[A_6^- - \Phi_1\vartheta_o A_3^- - \left\{A_4^- + \left(R - \frac{\Phi_2}{2}\right) A_1^- - \frac{\Phi_2\vartheta_o}{2} A_2^-\right\} \sin\vartheta_o\right.$$

$$- \left\{A_5^- + \left(R - \frac{\Phi_2}{2}\right) A_2^- + \frac{\Phi_2\vartheta_o}{2} A_1^-\right\} \cos\vartheta_o \quad - \delta\left[\left\{A_4^- + \frac{\Phi_2}{2} A_1^-\right.\right.$$

$$\left.\left. - \frac{\Phi_2\vartheta_o}{2} A_2^-\right\} \sin\vartheta_o + \left\{A_5^- + \frac{\Phi_2}{2} A_2^- + \frac{\Phi_2\vartheta_o}{2} A_1^-\right\} \cos\vartheta_o\right] = 0 \tag{140}$$

tangential displacement at $\vartheta = +\vartheta_o$ is zero:

$$(1 - \delta)\left[A_6^+ + \Phi_1\vartheta_o A_3^+ + \left\{A_4^+ + \left(R - \frac{\Phi_2}{2}\right) A_1^+ + \frac{\Phi_2\vartheta_o}{2} A_2^+\right\} \sin\vartheta_o\right.$$

$$- \left\{A_5^+ + \left(R - \frac{\Phi_2}{2}\right) A_2^+ - \frac{\Phi_2\vartheta_o}{2} A_1^+\right\} \cos\vartheta_o \quad - \delta\left[-\left\{A_4^+ + \frac{\Phi_2}{2} A_1^+\right.\right.$$

$$\left.\left. + \frac{\Phi_2\vartheta_o}{2} A_2^+\right\} \sin\vartheta_o + \left\{A_5^+ + \frac{\Phi_2}{2} A_2^+ - \frac{\Phi_2\vartheta_o}{2} A_1^+\right\} \cos\vartheta_o\right] = 0 \tag{141}$$

moment at $\vartheta = -\vartheta_o$ is zero:

$$\left\{A_5^- + \Phi_2 A_2^- + \frac{\Phi_2\vartheta_o}{2} A_1^-\right\} \sin\vartheta_o - \left\{A_4^- + \Phi_2 A_1^- - \frac{\Phi_2\vartheta_o}{2} A_2^-\right\} \cos\vartheta_o$$

$$+ (1 + \nu)\left[\Phi_1 A_3^- - \left\{A_5^- + RA_2^- + \frac{\Phi_2\vartheta_o}{2} A_1^-\right\} \sin\vartheta_o\right.$$

$$\left. + \left\{A_4^- + RA_1^- - \frac{\Phi_2\vartheta_o}{2} A_2^-\right\} \cos\vartheta_o\right] = 0 \tag{142}$$

moment at $\theta = +\theta_o$ is zero:

$$- \left\{ A_5^+ + \phi_2 A_2^+ - \frac{\phi_2 \theta_o}{2} A_1^+ \right\} \sin \theta_o - \left\{ A_4^+ + \phi_2 A_1^+ + \frac{\phi_2 \theta_o}{2} A_2^+ \right\} \cos \theta_o$$

$$+ (1 + \lambda) \left[\phi_1 A_3^+ + \left\{ A_5^+ + R A_2^+ - \frac{\phi_2 \theta_o}{2} A_1^+ \right\} \sin \theta_o \right.$$

$$\left. + \left\{ A_4^+ + R A_1^+ + \frac{\phi_2 \theta_o}{2} A_2^+ \right\} \cos \theta_o \right] = 0 \qquad (143)$$

continuity of radial displacements at $\theta = \psi$:

$$\phi_1 A_3^- + \left\{ A_5^- - \frac{\phi_2 \psi}{2} A_1^- \right\} \sin \psi + \left\{ A_4^- + \frac{\phi_2 \psi}{2} A_2^- \right\} \cos \psi =$$

$$\phi_1 A_3^+ + \left\{ A_5^+ - \frac{\phi_2 \psi}{2} A_1^+ \right\} \sin \psi + \left\{ A_4^+ + \frac{\phi_2 \psi}{2} A_2^+ \right\} \cos \psi \qquad (144)$$

continuity of tangential displacements at $\theta = \psi$:

$$A_6^- + \phi_1 \psi A_3^- + \left\{ A_4^- + \left(R - \frac{\phi_2}{2} \right) A_1^- + \frac{\phi_2 \psi}{2} A_2^- \right\} \sin \psi$$

$$- \left\{ A_5^- + \left(R - \frac{\phi_2}{2} \right) A_2^- - \frac{\phi_2 \psi}{2} A_1^- \right\} \cos \psi =$$

$$A_6^+ + \phi_1 \psi A_3^+ + \left\{ A_4^+ + \left(R - \frac{\phi_2}{2} \right) A_1^+ + \frac{\phi_2 \psi}{2} A_2^+ \right\} \sin \psi$$

$$- \left\{ A_5^+ + \left(R - \frac{\phi_2}{2} \right) A_2^+ - \frac{\phi_2 \psi}{2} A_1^+ \right\} \cos \psi \qquad (145)$$

continuity of rotations of $\theta = \psi$:

$$- \left\{A_4^- + \frac{\phi_2}{2} A_1^- + \frac{\phi_2\psi}{2} A_2^-\right\} \sin\psi + \left\{A_5^- + \frac{\phi_2}{2} A_2^- - \frac{\phi_2\psi}{2} A_1^-\right\} \cos\psi =$$

$$- \left\{A_4^+ + \frac{\phi_2}{2} A_1^+ + \frac{\phi_2\psi}{2} A_2^+\right\} \sin\psi + \left\{A_5^+ + \frac{\phi_2}{2} A_2^+ - \frac{\phi_2\psi}{2} A_1^+\right\} \cos\psi \tag{146}$$

jump in membrane force at $\theta = \psi$:

$$A_2^- \sin\psi + A_1^- \cos\psi + \frac{P \sin\alpha}{A_{22}} = A_2^+ \sin\psi + A_1^+ \cos\psi \tag{147}$$

continuity of moment at $\theta = \psi$:

$$\phi_1 A_3^- + (R - \phi_2)A_2^- \sin\psi + (R - \phi_2)A_1^- \cos\psi =$$

$$\phi_1 A_3^+ + (R - \phi_2)A_2^+ \sin\psi + (R - \phi_2)A_1^+ \cos\psi \tag{148}$$

jump in shear force at $\theta = \psi$:

$$- (R - \phi_2)A_1^- \sin\psi + (R - \phi_2)A_2^- \cos\psi + \phi_1 P \cos\alpha =$$

$$- (R - \phi_2)A_1^+ \sin\psi + (R - \phi_2)A_2^+ \cos\psi \quad . \tag{149}$$

Equations 138-149 are simply a set of linear algebraic equations of the form

$$\left[\ C\ \right] \left\{ \begin{matrix} A_1^- \\ A_2^- \\ A_3^- \\ A_4^- \\ A_5^- \\ A_6^- \\ A_1^+ \\ A_2^+ \\ A_3^+ \\ A_4^+ \\ A_5^+ \\ A_6^+ \end{matrix} \right\} = \left\{ \begin{matrix} B_1 \\ B_2 \\ B_3 \\ B_4 \\ B_5 \\ B_6 \\ B_7 \\ B_8 \\ B_9 \\ B_{10} \\ B_{11} \\ B_{12} \end{matrix} \right\} \qquad (150)$$

These can easily be solved for A_1^- through A_6^+. The Appendix gives the coefficients C_{ij} and B_j, i,j = 1,12.

Given the cylinder geometry, the material properties, and the loading condition, the matrix C and the vector B can be defined and coefficients A_1^- through A_6^+ can be computed. Once these coefficients are known, the deformed shape, the strains, the membrane force, the bending moment, the boundary reactions, and any other quantity related to the response can be determined. The next section presents numerical results regarding the response.

4. NUMERICAL RESULTS

Figure 6 shows the predicted stiffness characteristics of three 4-layer cylindrical panels as a function of panel geometry. The panels are assumed to be fabricated from glass-epoxy with the following material properties:

$$E_1 = 20.0 \times 10^6$$

$$E_2 = 1.04 \times 10^6$$

$$G_{12} = 1.50 \times 10^6$$

$$\nu_{12} = 0.28$$

$$t = 0.005 \text{ in. (lamina thickness)}$$

The case shown in Fig. 6 is for panels with the line load exactly at mid-span ($\psi = 0$) and aligned radially ($\alpha = 0$). The stiffness 'K' is defined as the total load divided by the radial deflection under the load. The stiffness has been normalized by the stiffness of a pinned-end panel with a symmetric $[90/0/0/90]_T$ stacking arrangement and with a semi-opening angle of π (see Eq. B.9 in Appendix B). The pinned-end panel with semi-opening angle of π is not be be confused with a closed ring. The difference is illustrated below.

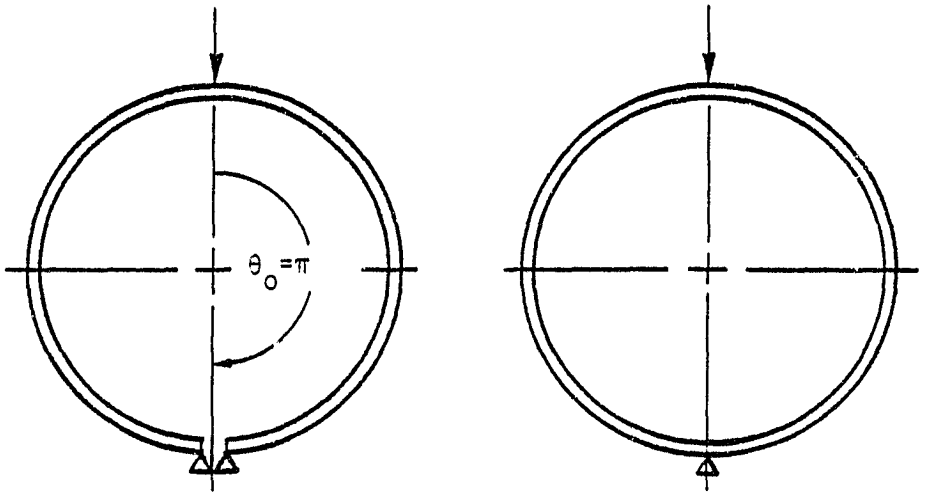

pinned-end panel with semi-opening angle π

closing ring

The notation on stacking sequence needs some explanation. The notation reads from the left to the right, for example in $[90/0/0/90]_T$, and each number is associated with a particular lamina. The number indicates the angle of the fibers in the lamina relative to the global x-axis. The left most entry in the stacking sequence notation refers to the lamina at the negative most z position. Reading to the right in the notation corresponds to moving from lamina to lamina in the direction of positive z. Thus, for the problem here, $[90/0/0/90]_T$ signifies that the fibers in the innermost and the outermost lamina are in the circumferential direction while the fibers in the two inner lamina are in the generator direction.

In Fig. 6 the abscissa is the scaled semi-opening angle θ_o/π. This parameter completely characterizes the panel's depth, or "bulge," with respect to the chord line connecting the support points. It can be seen from Fig. 1. that this rise to span ratio for the panel is

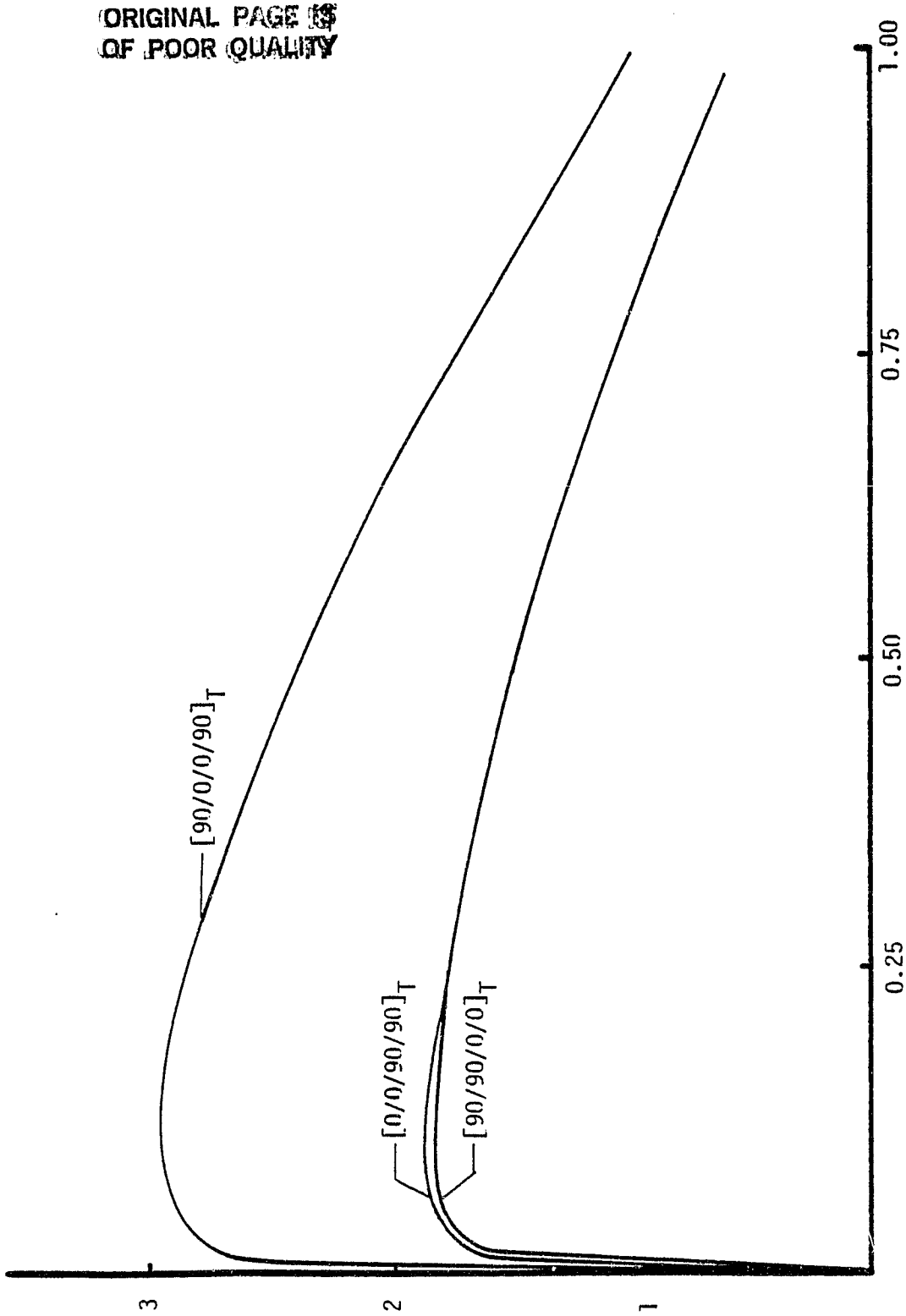

Fig. 6 Stiffness Characteristics of Cylindrical Panels of Various Stacking Arrangements

$$\frac{H}{L} = \frac{1}{2}\frac{(1-\cos\theta_o)}{\sin\theta_o} \quad . \tag{151}$$

Thus, as stated, the semi-opening angle completely characterizes the panel's depth. Moreover, Eq. 151 implies that for a shallow panel in which the rise to span is small that θ_o is small, i.e.,

$$\frac{H}{L} \sim \frac{1}{4}\theta_o, \text{ for } \theta_o \text{ small.} \tag{152}$$

Shallowness means a small semi-opening angle, independent of the panel's radius.

Figure 6 shows the stiffness characteristics of a $[90/0/0/90]_T$ panel, a $[0/0/90/90]_T$ panel and a $[90/90/0/0]_T$ panel. The first panel represents a symmetric stacking arrangement that can be made using ordinary fabrication techniques, i.e. laying the prepreg over the cylindrical mandrel and curing it. The second panel represents an unsymmetric lay-up that would naturally assume the cylindrical shape if it were fabricated flat, cured, and cooled. The third panel is a fictious unsymmetric panel which if actually fabricated would have curvature characteristics opposite to that implied in Fig. 1. This panel was studied only to assess the effects of the through-the-thickness location of the circumferential fibers. It is important to note that all of the panels in Fig. 6, and in subsequent discussions, have an equal volume of material (arc-length of 20 inches). Thus, in a sense, material efficiency is being studied.

From Fig. 6 it appears that the symmetric panel affords the stiffest configuration, except when the opening angle is small. The stiffnesses of the two unsymmetric panels are identical. The small opening angle region will be referred to as the shallow panel case. Before this study began, it was not clear whether the unsymmetrically laminated panel would be softer than the symmetric counterpart. If membrane forces governed the stiffness, perhaps the stacking arrangement was not important. If bending forces governed the stiffness, then the stacking arrangement would be important. With a $[90/0/0/90]_T$ configuration, the circumferential fibers are in the best position, through-the-thickness, for resisting bending. In the other stacking arrangements the circumferential fibers are all on one side or the other of the bending axis. Thus it appears bending stiffness is quite important, at least for deep panel configurations.

To obtain a more detailed comparison of the stiffness when shallow panels are considered, the stiffness and geometric perameters are rescaled. The stiffness is nondimensionalized by the stiffness, K_b, of a $[90/0/0/90]_T$ simply supported beam (see Eq. B.20 Appendix B) and the ratio of the panel rise to laminate thickness is used to describe the deviation from a flat configuration. Figure 7 shows a comparison of the 3 panels for the case of shallow panels. The figure has several interesting features. First, it is obvious a slight curvature in a 'beam' dramatically increases the stiffness. For a rise-to-thickness ratio of even 1, the stiffness has increased several times. This phenomena is not unique to composites. It happens with metals and the increased stiffness is due to geometric effects. The second feature to

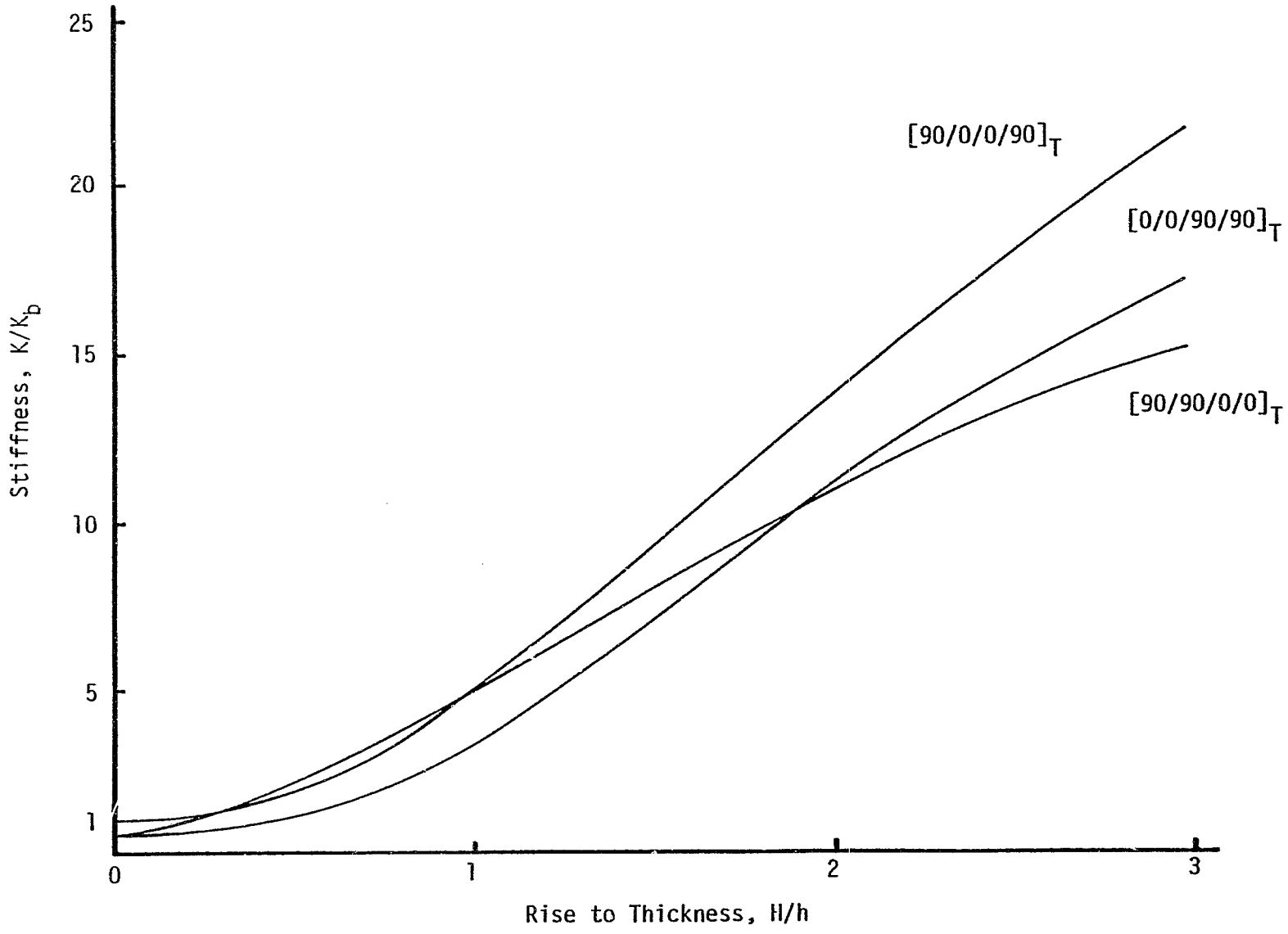

Fig. 7 Stiffness Characteristics of Shallow Panels

be noted is that for a small range of rise-to-thickness ratios, the unsymmetric $[90/90/0/0]_T$ panel is stiffer than the symmetric panel. Above a rise-to-thickness ratio of about 1, the $[90/90/0/0]_T$ is always less stiff than the symmetric panel. The ratio of the stiffness for each unsymmetric flat panel to the stiffness of the symmetric flat panel is 0.545, which may be determined from Eqs. B.19 and B.20 in Appendix B.

For a shallow panel, the induced membrane force is a significant component of the panel's stiffness. This membrane effect adds to the inherent bending stiffness. Thus the membrane force at the pinned support was examined. For the loading here the membrane force was compressive, or a thrust, and Fig. 8 shows how it varies with panel geometry for the 3 different stacking arrangements. From the figure it is clear that even though the bending stiffness of an unsymmetric panel is less than the bending stiffness of the symmetric ones, the induced thrust in an unsymmetric panel can be greater. In the case of the $[90/90/0/0]_T$ panel this increased thrust increases the global stiffness beyond the symmetric panel's. The figure also indicates that the deeper the panel, the less is the difference in thrust among laminates. As suggested by Fig. 8, the thrust has significantly less contribution to the global stiffness for the deeper panels.

It is interesting to determine if the shallowness approximation (θ_0 small) is influenced by the laminate configuration. For metallic panels shallowness is determined solely by geometry, see Eq. 152. The error in the shallowness approximation on panel stiffness is shown in Fig. 9 as a function of the scaled semi-opening angle θ_0/π. Panel stiffness as

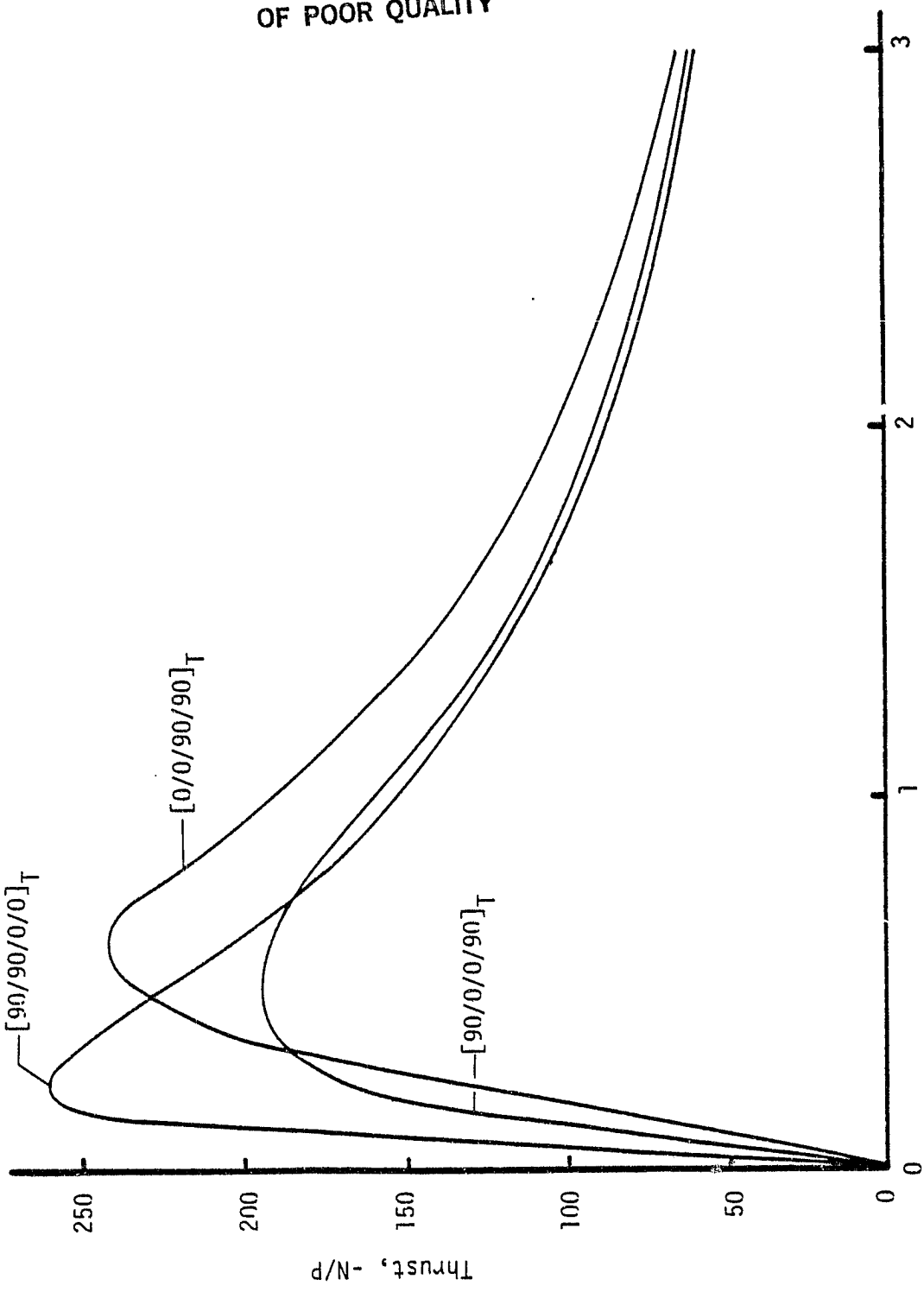

Fig. 8 Thrust Versus Rise for Shallow Panels

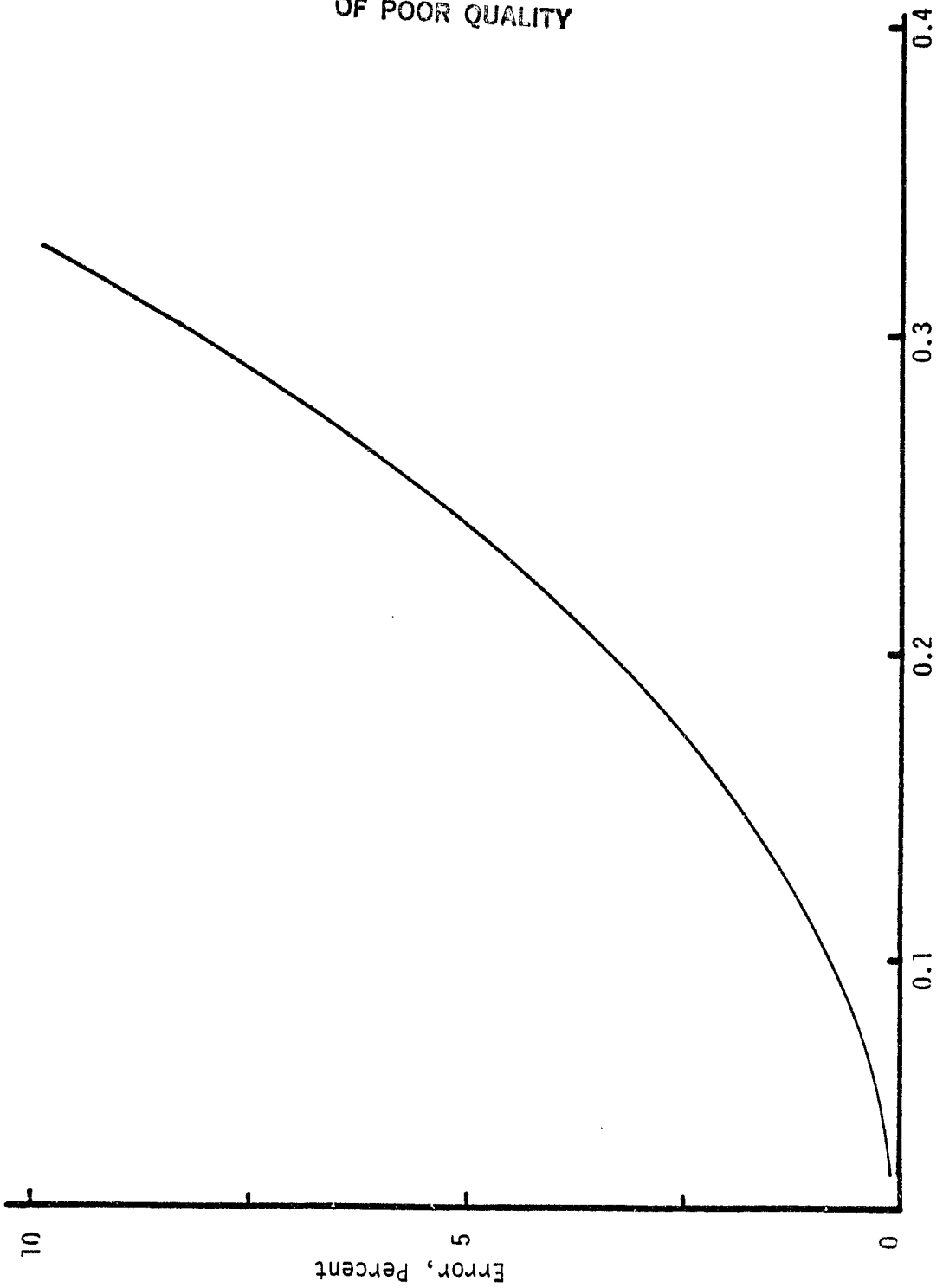

Fig. 9 Error in the Shallowness Approximation for Panel Stiffness

computed from the assumption of shallowness is designated K_{sh} and is derived in Appendix B (see Eqs. B.10 to B.17). The percent error on the ordinate of Fig. 9 is defined as

$$\varepsilon = (K_{sh}/K-1)100,$$

in which K denotes the exact panel stiffness from the general theory (θ_o arbitrary). For the resolution on the graph shown in Fig. 9, the differences between the error curves for the $[90/0/0/90]_T$, $[90/90/0/0]_T$, and $[0/0/90/90]_T$ laminates are indistinguishable. Hence shallowness is essentially unaffected by lamination dissymmetry, and thus, it truely is a geometric quantity.

Of fundamental importance to the integrity of composite structures is the strain levels. Due to the brittleness of epoxies, large tensile strains in the matrix direction of the epoxy matrix laminates cannot be tolerated. Even if adjacent layers have the ability to hold the structure together, cracks in lamina are simply bad. A crack in one lamina can induce cracking in an adjacent lamina even though the cracks could ultimately be at right angles to each other. Cracking can lead to delamination and the problems inherent with that sort of damage. Thus it is important to assess the strain levels in these three laminates. Figure 10 shows the circumferential strains in the three laminates.

The maximum circumferential strains at the innermost and outermost radial location were computed as a function of panel geometry. The outermost strain's were compressive while the innermost strains were tensile. The maximum strain's occurred at the load location. In the

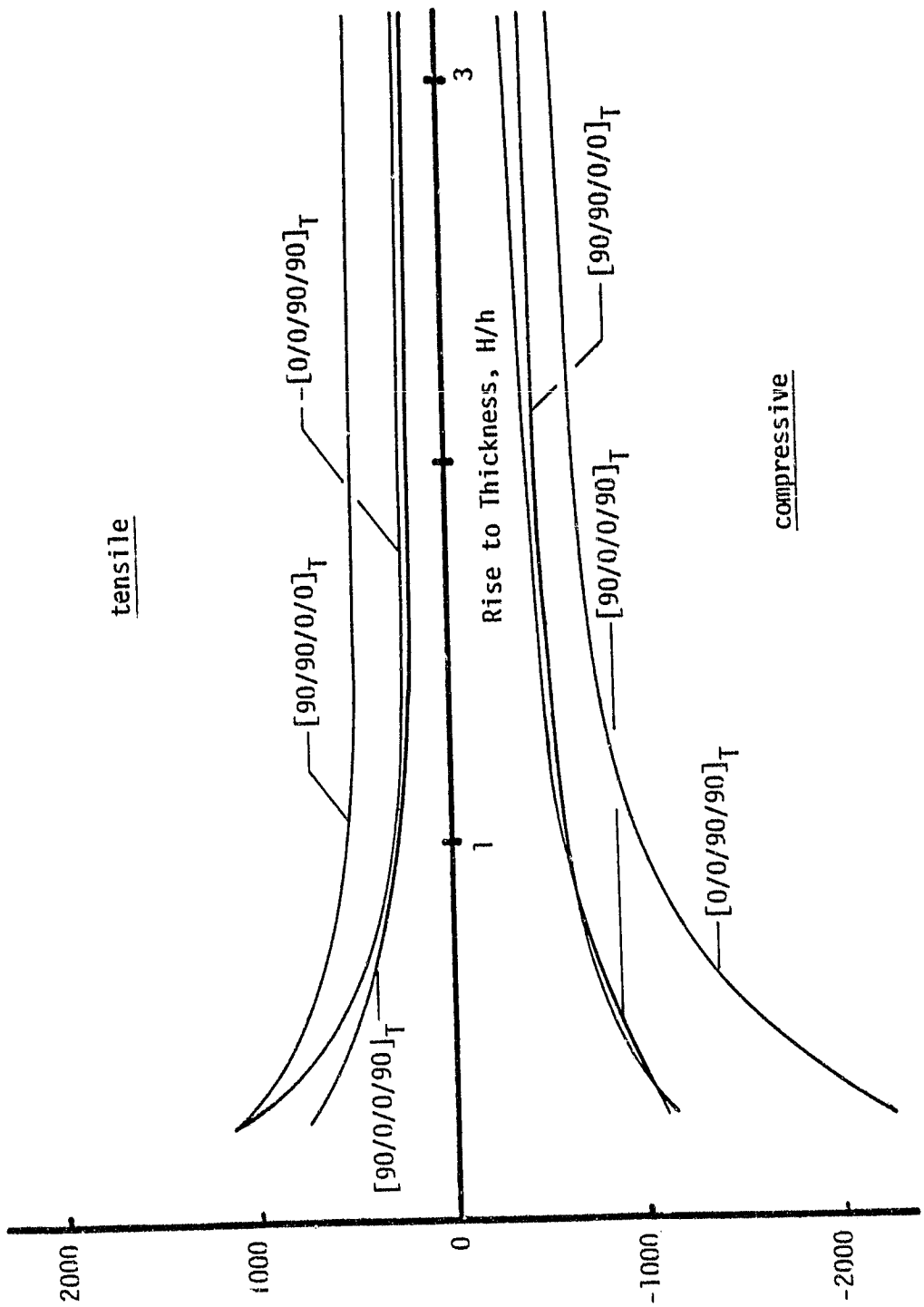

Fig. 10 Maximum Circumferential Strain in Cylindrical Panels

symmetric laminate, the circumferential fibers in the inner and outer plys react these maximum strains. In the $[90/90/0/0]_T$ the inner tensile strains are reacted by matrix while the outer compressive strains are reacted by fibers. In the $[0/0/90/90]_T$ the tensile strains are reacted by the fibers while the compressive strains are reacted by the matrix.

As can be seen in Fig. 10, the $[90/90/0/0]_T$ laminate yields the largest tensile strains while the $[0/0/90/90]_T$ laminate produces the largest compressive strains. Shallowness appears to have much to do with the magnitude of the strains on the opposite sides of the panel. As the panels become deep (H/h increasing) the strains on opposite sides become nearly equal in magnitude, an indication of bending effects dominating.

The results presented so far have been for the case where the load is actually radial and it is located exactly at midspan. This is an ideal situation. In practice it is difficult to achieve the symmetry in the loading implied by this situation. Oftentimes the load is slightly rotated ($\alpha \neq 0$) relative to the radial lines so that it does not act entirely in a radial direction. In addition, the load may not be exactly at midspan ($\psi \neq 0$), acting a little to one side or the other of the geometric center of the panel. In some structures such deviations from the ideal loading can cause a response that is drastically different than the response to the ideal case, even if the deviation is small. This is particularly true for imperfection sensitive structures which exhibit a significant decrease in the static buckling load of the perfect structure for small eccentricities in the load position or for small geometric imperfections in the structure's initial shape. For

example, an elastic arch with symmetric end conditions and unloaded shape, subjected to a downward point load at midspan, is imperfection sensitive if the arch rise is sufficiently large to cause instability at a bifurcation point [5]. Thus the sensitivity of the cylindrical panels, particularly the unsymmetrically laminated ones, to deviations from the ideal loading case was studied. The stiffness of the panels was again used as an indicator of panel response. If the load is rotated slightly relative to the radial direction, not all of the deflection is radial. However, the stiffness was still defined as the total load divided by the radial deflection under the load. The reason for this definition of stiffness is that if experimentally one was determining the stiffness and did not realize that the load was rotated, this definition would still be used to compute stiffness.

In what follows, the stiffnesses for the nonideal cases have been normalized by the stiffness for the ideal $[90/0/0/90]_T$ case. The stiffnesses will be assumed to be a function of the location of the load, ψ, and the inclination of the load, α. Thus, the notation $\kappa = \kappa(\psi,\alpha)$. The ideal case will be donated as $\kappa(\psi=0,\alpha=0)$. Figure 11 shows the stiffness of a typical shallow panel (R = 100 in., θ_0/π = 0.032) as a function of the location of the load along the span of the panel. The load is assumed to act radially (α = 0). Figures depicting the effects of load location and orientation can become cluttered if, in addition, various panel geometries are shown. Thus a single panel geometry representative of a shallow panel was chosen. As can be seen in the figure, slight deviations of load locations from the center positions cause no noticable decrease in stiffness. As the load location reaches quarter-span, ψ/θ_0 = 0.5, the stiffness decreases considerably.

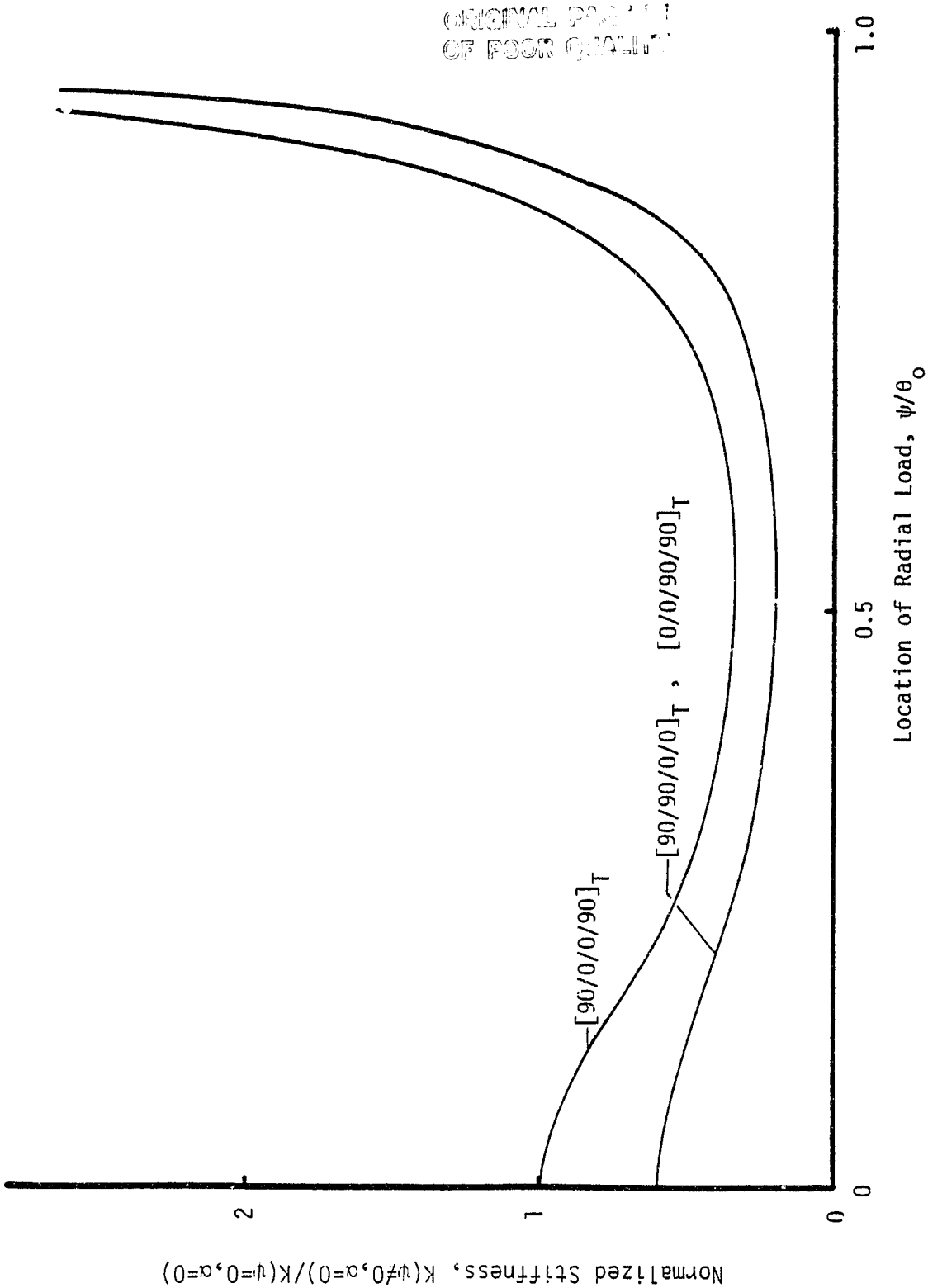

Fig. 11 Sensitivity of Panel Stiffness to Location of Radial Load (R=100 in., θ_o/π=0.032)

As the point of application of the load approaches the support, ψ/θ_o = 1, the stiffness becomes very large. The stiffness variations of both unsymmetric laminates and the symmetric one are similar and there are no adverse sensitivity problems with the unsymmetric laminates. In essence, if the load were not exactly at midspan in an experiment, the stiffness calculations would not be in error. Figure 12 shows the stiffness characteristics of a deep panel (R = 6.5 in., θ_o/π = 0.5) as a function of load location. Again, there does not appear to be any adverse sensitivity for any laminate.

Figures 13 and 14 show the effect on stiffness of a rotation of the load from the purely radial inclination. Figure 13 is for a representative shallow panel (R = 100 in., θ_o/π = 0.032) and the load is assumed to act at midspan (ψ = 0). It is clear that for inclinations 15° - 20° from the radial direction, the increase in stiffness over the ideal case is negligible. As the load rotates more and more from the radial position it begins to encounter the membrane effect of the panel and the radial deflections decrease. The unsymmetrically laminated panels seem to have the same characteristic as the symmetric panel. In addition, as shown in Fig. 14, the deeper panels behave similarly.

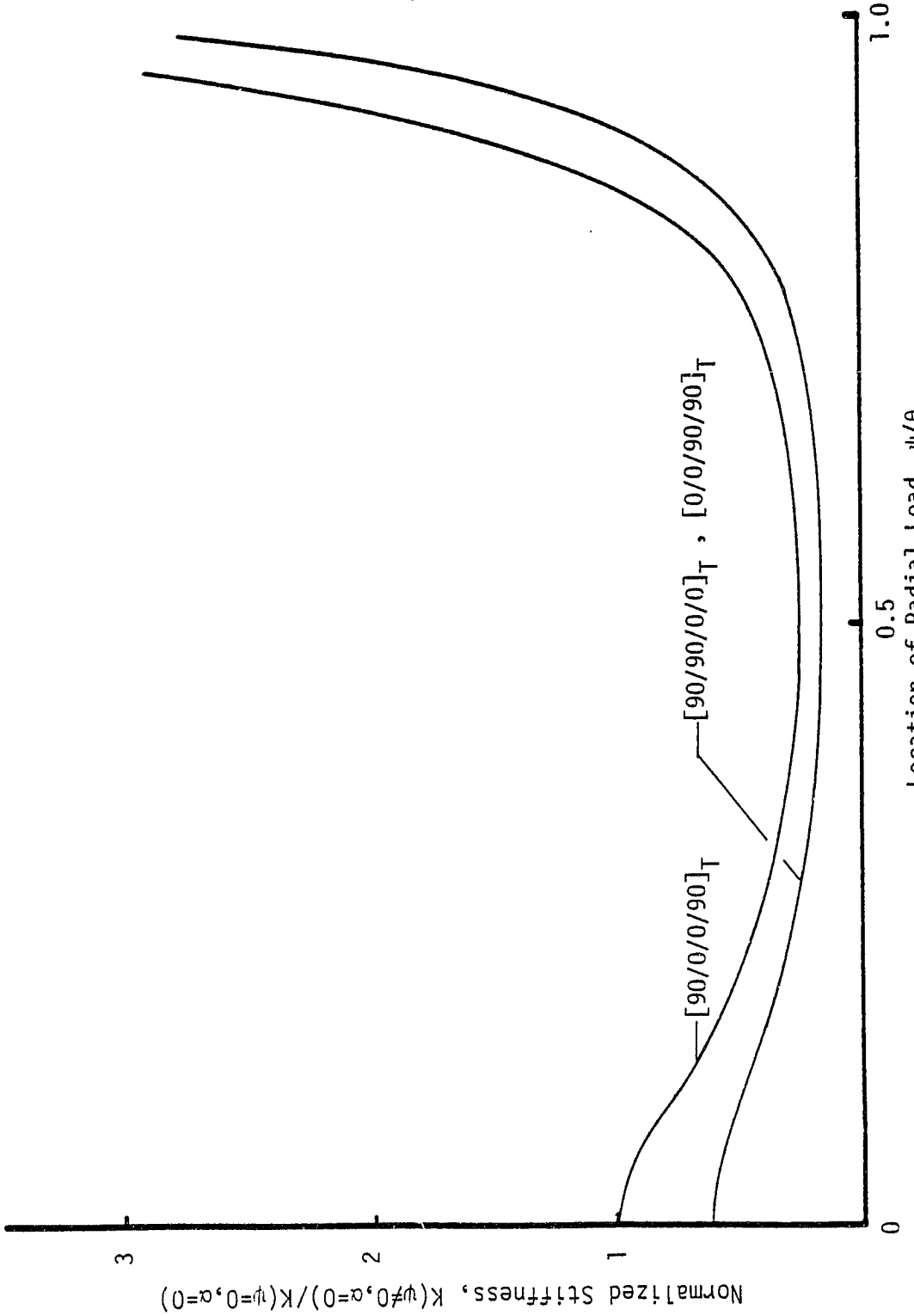

Fig. 12 Sensitivity of Panel Stiffness to Location of Radial Load (R=6.5 in., θ_o/π=0.5)

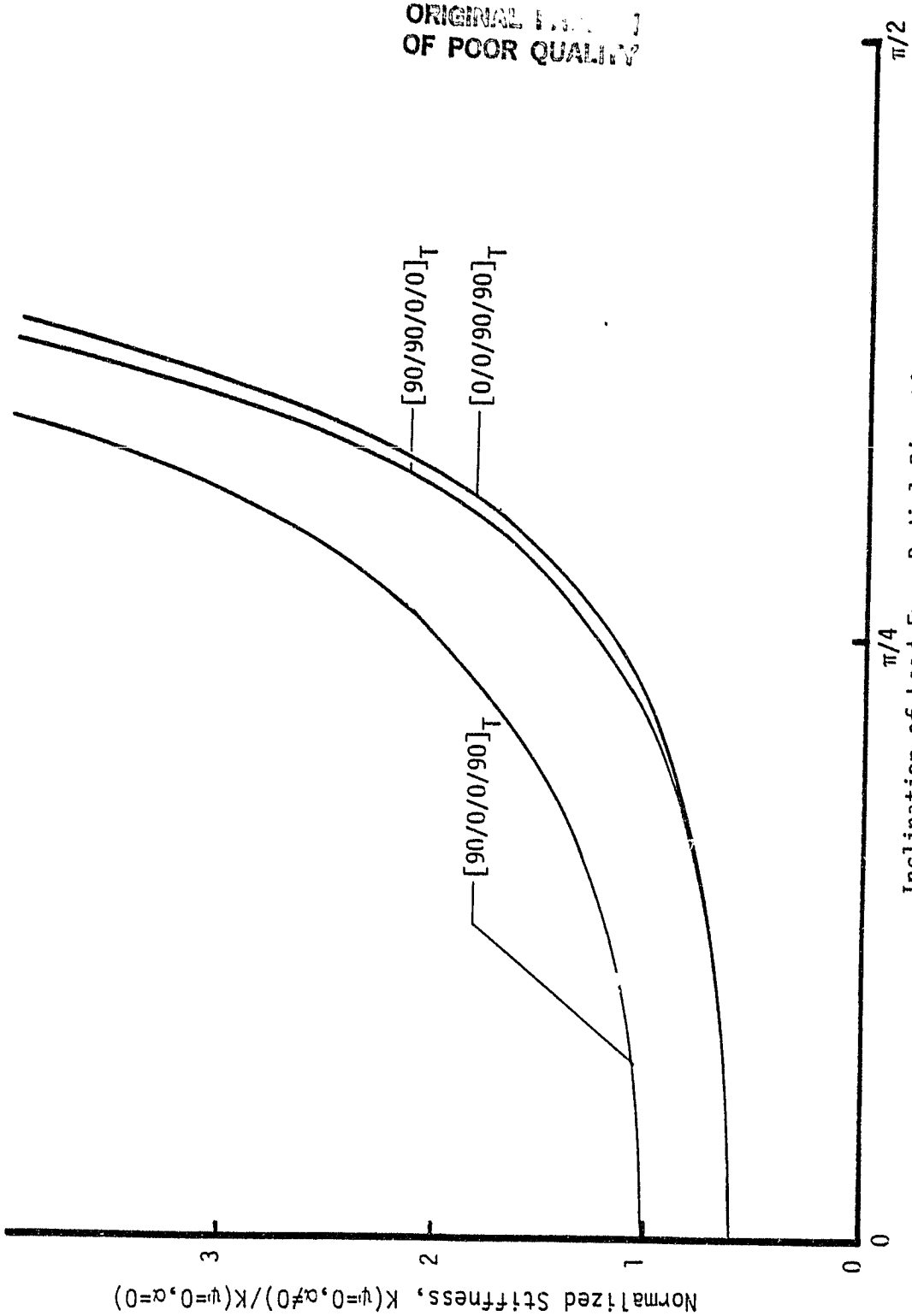

Fig. 13 Sensitivity of Panel Stiffness to Load Inclination (R=100 in., θ_o/π=0.032)

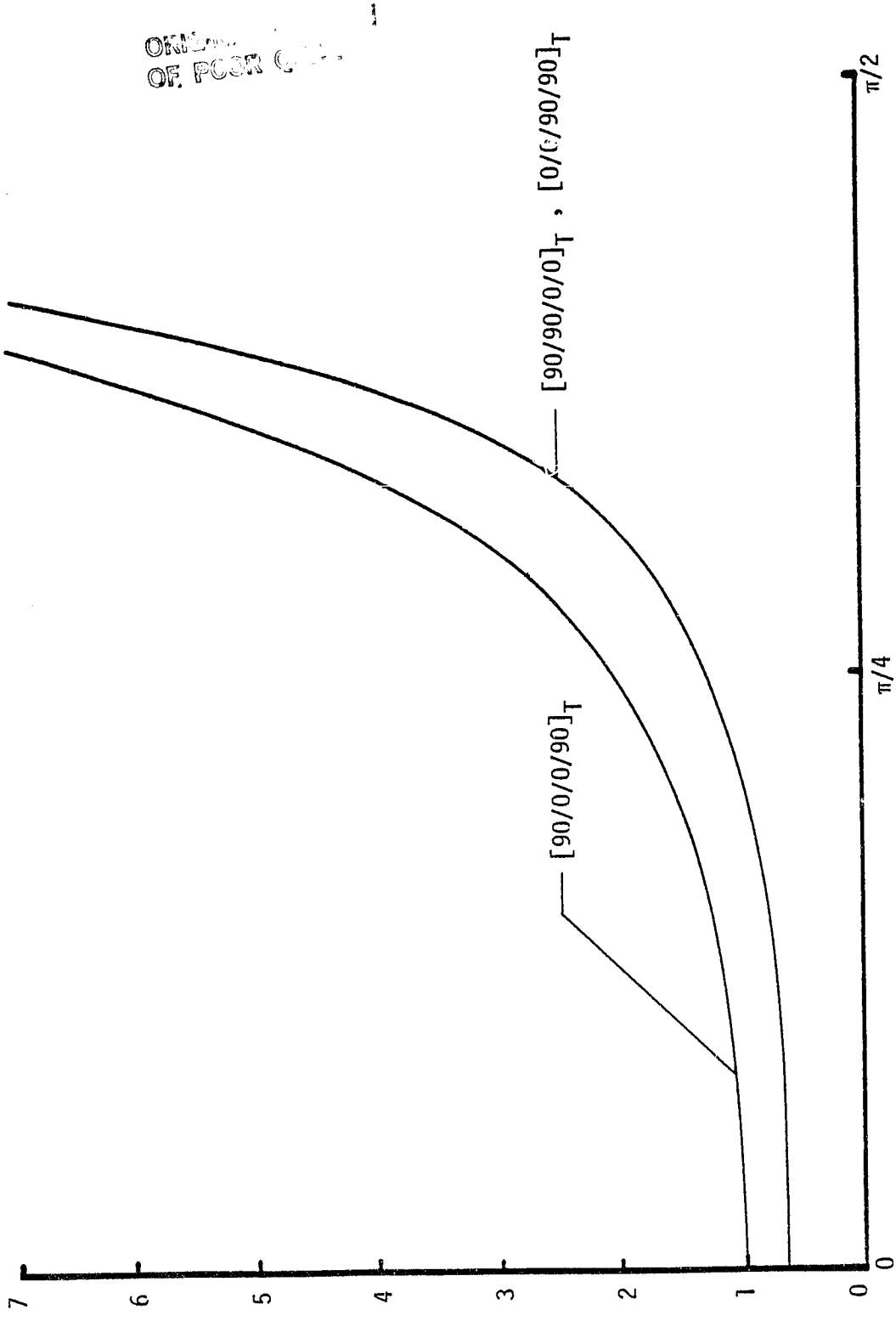

Fig. 14 Sensitivity of Panel Stiffness to Load Inclination (R=6.5 in., θ_o/π=0.5)

5. A LIMITED COMPARISON WITH EXPERIMENTAL RESULTS

To determine if the predictions of the response of unsymmetrically laminated cylindrical panels were correct, a $[0_4/90_4]_T$ T300/5208 graphite-epoxy cylindrical panel was fabricated. In the uncured state the flat panel was 12 x 12 in. When cured, the panel had a radius of curvature of 10.2 in. The panel was fabricated at the Air Force Materials Laboratory, Wright-Patterson Air Force Base. The authors extend their appreciation to Stephen W. Tsai for providing for the panel fabrication.

The panel was mounted horizontally, the panel midspan being higher than the supported ends. The pin supports were simulated by using two steel right-angle members parallel to the generator direction and running the length of the cylinder. The open side of each angle member was towards the panel. One leg of each angle member was horizontal and the other leg was vertical. Each straight edge of the panel was seated in the corner of a right-angle. The angles were clamped so they could not move relative to one another. The vertical leg of each angle prevented the cylindrical panel from spreading as a downward load was applied. The horizontal legs provided a vertical reaction to the applied downward load. Dead weights acting on a stiff bar that ran the length of the cylinder provided the line load. The load acted radially ($\alpha = 0$) at the panel midspan ($\theta = 0$). The results of Figs. 11-15 indicated that the panel response would not be overly sensitive to slightly off-center ($\theta \neq 0$) or slightly misaligned loads ($\alpha \neq 0$). Figure 15 shows the setup. Dial gages were used to monitor the radial deflections of the cylinder at several locations.

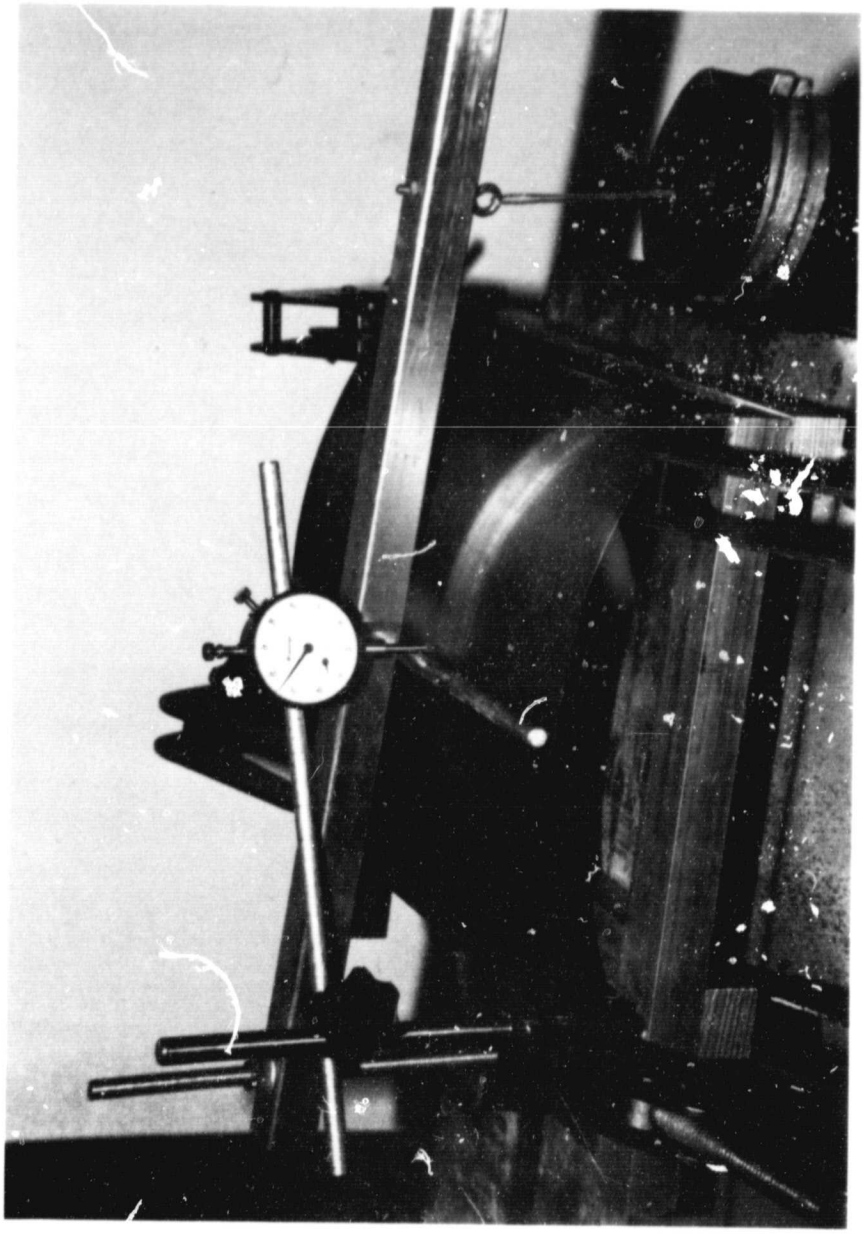

Fig. 15 Set-Up for Loading Cylinders

Figure 16 shows the load deflection characteristics of the panel. The experiment was terminated after the panel deflected more than 4 laminate thicknesses simply because this was felt to be the range of the linear theory developed here. The correlation is not particularly good. To put the results in context, a $[(90/0)_2]_S$ T300/5208 graphite-epoxy cylindrical panel with a 12-inch radius was tested. The panel was obtained from the Air Force Flight Dynamics Laboratory and the authors extend their appreciation to Capt. Marvin Becker for providing the panel. The panel had been previously buckled with inplane compressive loads acting in the generator direction. There was no noticeable damage to the panel from the previous buckling. Figure 17 shows the symmetric panel and the unsymmetric panel side-by-side. Figure 18 shows the load-deflection characteristics of the symmetric panel. Again the correlation is not good. In fact, the correlation for the symmetric panel is worse than the correlation for the unsymmetric panel. It is not entirely clear why the correlation for both panels is not better. Some overstiffness is expected in the predictions but not to the degree observed here.

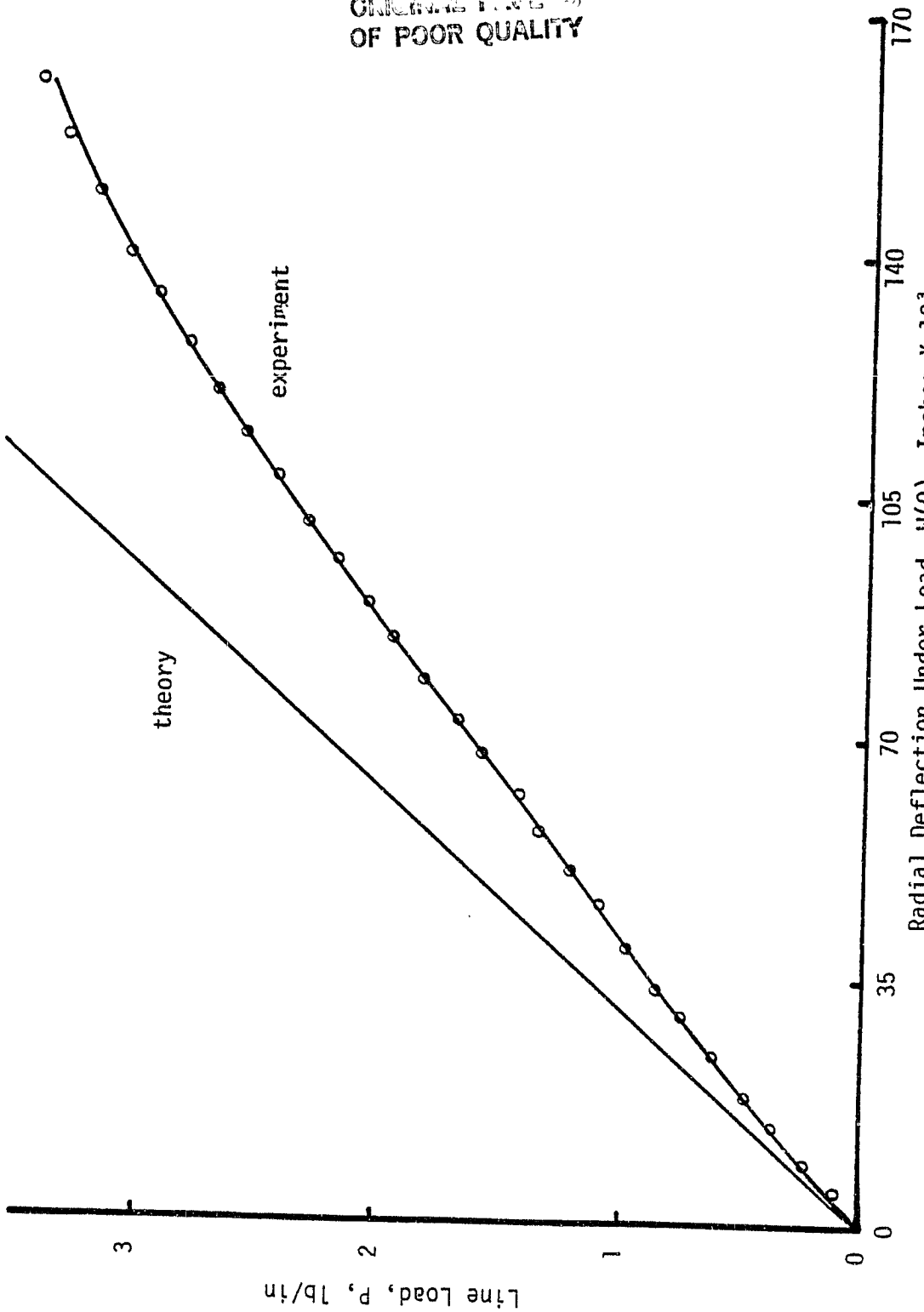

Fig. 16 Load-Deflection Characteristics of Unsymmetric Panel

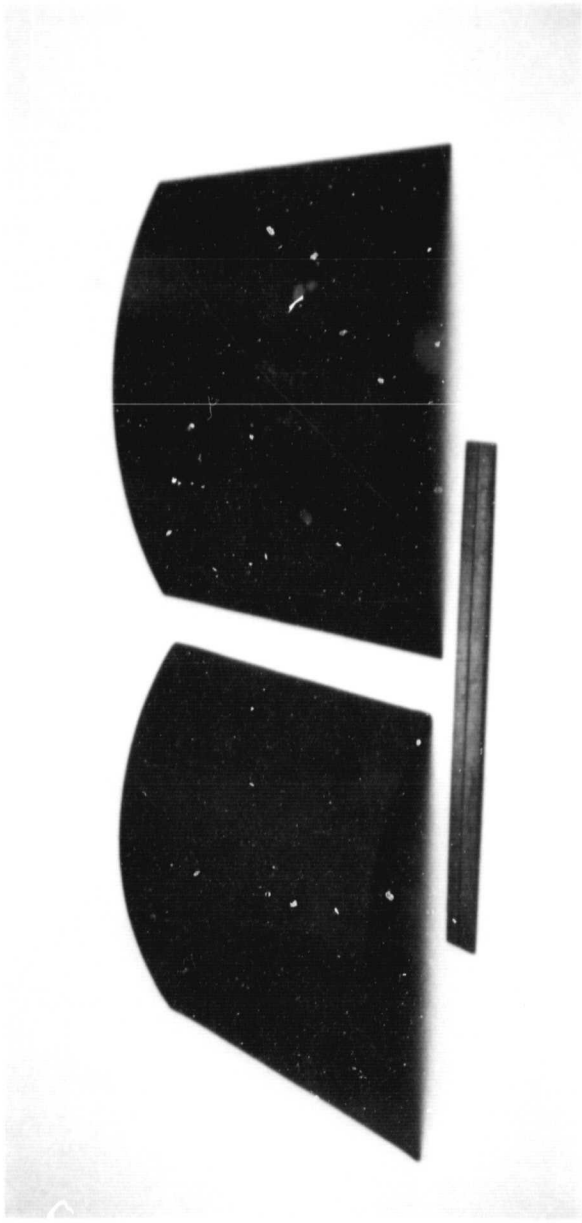

Fig. 17 Unsymmetrically (Left) and Symmetrically (Right) Laminated Cylinders

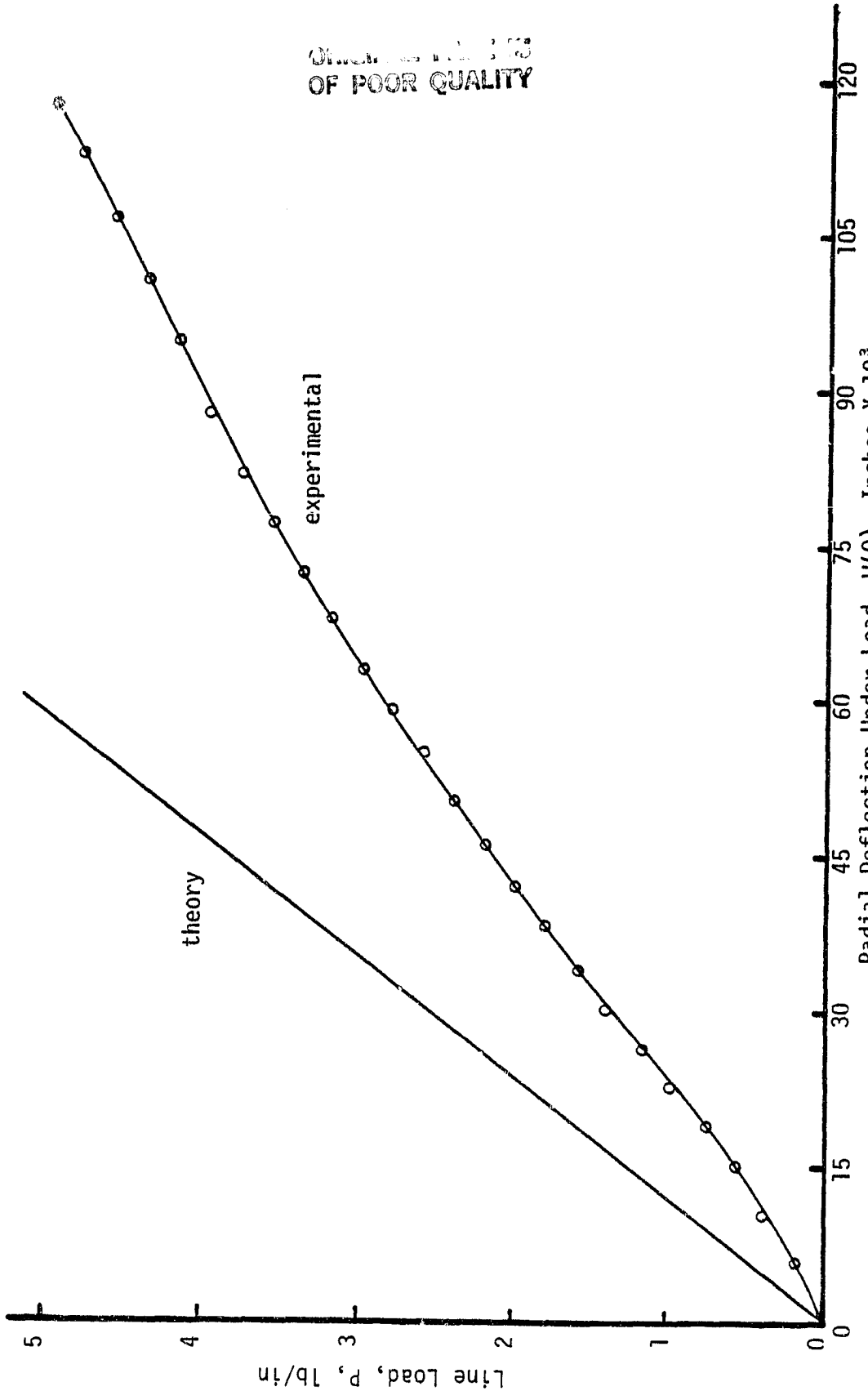

Fig. 18 Load-Deflection Characteristics of Symmetric Panel

REFERENCES

1. Jones, R. M., Mechanics of Composite Materials, McGraw-Hill Book Co., New York, NY (1975).

2. Tsai, S. W. and Hahn, H. T., Introduction to Composite Materials, Technomic Publishing Co., Westport, CT (1980).

3. Hyer, M. W., "Some Observations on the Cured Shapes of Unsymmetrically Laminated Composites," Journal of Composite Materials, Vol. 15, p. 175-194 (1981).

4. Hyer, M. W., "Calculations on the Room Temperature Shapes of Unsymmetrically Laminated Composites," Journal of Composite Materials, Vol. 15, p. 296-310 (1981).

5. Plaut, Raymond H., "Influence of Load Position on the Stability of Shallow Arches," Journal of Applied Mathematics and Physics (ZAMP), Vol. 30, pp. 548-552 (1979).

APPENDIX A

Definition of Coefficients C_{ij} and B_j

Eq. 138

$$C_{1,1} = -\frac{\phi_2\theta_0}{2}\cos\theta_0$$

$$C_{1,2} = -\frac{\phi_2\theta_0}{2}\cos\theta_0$$

$$C_{1,3} = \phi_1$$

$$C_{1,4} = \cos\theta_0$$

$$C_{1,5} = -\sin\theta_0$$

$$C_{1,6} \rightarrow C_{1,12} = 0$$

$$B_1 = 0$$

Eq. 139

$$C_{2,1} \rightarrow C_{2,6} = 0$$

$$C_{2,7} = C_{1,1}$$

$$C_{2,8} = -C_{1,2}$$

$$C_{2,9} = C_{1,3}$$

$$C_{2,10} = C_{1,4}$$

$$C_{2,11} = -C_{1,5}$$

$$C_{2,12} = 0$$

$$B_2 = 0$$

Eq. 140

$$C_{3,1} = (1 - \delta)\left\{ - \left(R - \frac{\phi_2}{2}\right)\sin \theta_0 - \frac{\phi_2 \theta_0}{2} \cos \theta_0 \right\}$$

$$- \delta \left\{ \frac{\phi_2}{2} \sin \theta_0 + \frac{\phi_2 \theta_0}{2} \cos \theta_0 \right\}$$

$$C_{3,2} = (1 - \delta)\left\{ \frac{\phi_2 \theta_0}{2} \sin \theta_0 - \left(R - \frac{\phi_2}{2}\right) \cos \theta_0 \right\}$$

$$- \delta \left\{ - \frac{\phi_2 \theta_0}{2} \sin \theta_0 + \frac{\phi_2}{2} \cos \theta_0 \right\}$$

$$C_{3,3} = - (1 - \delta)\, \phi_1 \theta_0$$

$$C_{3,4} = - \sin \theta_0$$

$$C_{3,5} = - \cos \theta_0$$

$$C_{3,6} = 1 - \delta$$

$$C_{3,7} \rightarrow C_{3,12} = 0$$

$$B_3 = 0$$

Eq. 141

$$C_{4,1} \rightarrow C_{4,6} = 0 \qquad C_{4,7} = - C_{3,1}$$

$$C_{4,8} = C_{3,2} \qquad C_{4,9} = - C_{3,3}$$

$$C_{4,10} = - C_{3,4} \qquad C_{4,11} = C_{3,5}$$

$$C_{4,12} = C_{3,6} \qquad B_4 = 0$$

Eq. 142

$$C_{5,1} = (1 + \lambda)\left\{ - \frac{\phi_2\theta_0}{2} \sin \theta_0 + R \cos \theta_0 \right\} + \frac{\phi_2\theta_0}{2} \sin \theta_0 - \phi_2 \cos \theta_0$$

$$C_{5,2} = (1 + \lambda)\left\{ - R \sin \theta_0 - \frac{\phi_2\theta_0}{2} \cos \theta_0 \right\} + \phi_2 \sin \theta_0 + \frac{\phi_2\theta_0}{2} \cos \theta_0$$

$$C_{5,3} = (1 + \lambda)\, \phi_1$$

$$C_{5,4} = \lambda \cos \theta_0$$

$$C_{5,5} = -\lambda \sin \theta_0$$

$$C_{5,6} \rightarrow C_{5,12} = 0$$

$$B_5 = 0$$

Eq. 143

$$C_{6,1} \rightarrow C_{6,6} = 0$$

$$C_{6,7} = C_{5,1}$$

$$C_{6,8} = - C_{5,2}$$

$$C_{6,9} = C_{5,3}$$

$$C_{6,10} = C_{5,4}$$

$$C_{6,11} = - C_{5,5}$$

$$C_{6,12} = 0$$

$$B_6 = 0$$

Eq. 144

$$C_{7,1} = -\frac{\phi_2\psi}{2}\sin\psi \qquad C_{7,2} = \frac{\phi_2\psi}{2}\cos\psi$$

$$C_{7,3} = \phi_1 \qquad C_{7,4} = \cos\psi$$

$$C_{7,5} = \sin\psi \qquad C_{7,6} = 0$$

$$C_{7,7} = -C_{7,1} \qquad C_{7,8} = -C_{7,2}$$

$$C_{7,9} = -C_{7,3} \qquad C_{7,10} = -C_{7,4}$$

$$C_{7,11} = -C_{7,5} \qquad C_{7,12} = 0$$

$$B_7 = 0$$

Eq. 145

$$C_{8,1} = R - \frac{\phi_2}{2}\sin\psi + \frac{\phi_2\psi}{2}\cos\psi$$

$$C_{8,2} = \frac{\phi_2\psi}{2}\sin\psi - R - \frac{\phi_2}{2}\cos\psi \qquad C_{8,3} = \phi_1\psi$$

$$C_{8,4} = \sin\psi \qquad C_{8,5} = -\cos\psi \qquad C_{8,6} = 1 \qquad C_{8,7} = -C_{8,1}$$

$$C_{8,8} = -C_{8,2} \qquad C_{8,9} = -C_{8,3} \qquad C_{8,10} = -C_{8,4}$$

$$C_{8,11} = -C_{8,5} \qquad C_{8,12} = -C_{8,6} \qquad B_8 = 0$$

Eq. 146

$$C_{9,1} = -\frac{\phi_2}{2}\sin\psi - \frac{\phi_2\psi}{2}\cos\psi \qquad C_{9,2} = -\frac{\phi_2\psi}{2}\sin\psi + \frac{\phi_2}{2}\cos\psi$$

$$C_{9,3} = 0 \qquad C_{9,4} = -\sin\psi \qquad C_{9,5} = \cos\psi$$

$$C_{9,6} = 0 \qquad C_{9,7} = -C_{9,1} \qquad C_{9,8} = -C_{9,2}$$

$$C_{9,9} = 0 \qquad C_{9,10} = -C_{9,4} \qquad C_{9,11} = -C_{9,5}$$

$$C_{9,12} = 0 \qquad B_9 = 0$$

Eq. 147

$$C_{10,1} = \cos\psi \qquad C_{10,2} = \sin\psi \qquad C_{10,3} \rightarrow C_{10,6} = 0$$

$$C_{10,7} = -C_{10,1} \qquad C_{10,8} = -C_{10,2}$$

$$C_{10,9} \rightarrow C_{10,12} = 0 \qquad B_{10} = -\frac{P}{A_{22}}\sin\alpha$$

Eq. 148

$$C_{11,1} = (R - \phi_2)\cos\psi \qquad C_{11,2} = (R - \phi_2)\sin\psi \qquad C_{11,3} = \phi_1$$

$$C_{11,4} \rightarrow C_{11,6} = 0 \qquad C_{11,7} = -C_{11,1} \qquad C_{11,8} = -C_{11,6}$$

$$C_{11,9} = -C_{11,3} \qquad C_{11,10} \rightarrow C_{11,12} = 0 \qquad B_{11} = 0$$

Eq. 149

$$C_{12,1} = -(R - \phi_2)\sin\psi \qquad C_{12,2} = (R - \phi_2)\cos\psi$$

$$C_{12,3} \rightarrow C_{12,6} = 0 \qquad C_{12,7} = -C_{12,1}$$

$$C_{12,8} = -C_{12,2} \qquad C_{12,9} \rightarrow C_{12,12} = 0$$

$$B_{12} = -\frac{R^3 P}{D_{22}}\cos\alpha$$

APPENDIX B

Panel Stiffness by Castigliano's Theorem

The global panel stiffness may be obtained with relatively few algebraic manipulations by Castigliano's second theorem for some special geometric configurations if the line load P is directed radially inward at midspan ($\psi = \alpha = 0$ in Fig. 4). These manipulations are outlined in this appendix for the deepest panel ($\theta_o = \pi$), a very shallow panel (θ_o small), and a flat panel.

The complementary strain energy per unit length in the x-direction of the panel is

$$V = (\frac{1}{2}) \int_{-\theta_o}^{\theta_o} [\frac{M^2}{D_{22}} + \frac{N^2}{A_{22}}] R \, d\theta \, . \tag{B.1}$$

From appropriate free body diagrams of a circular cylindrical panel with arbitrary θ_o, the statically admissible force fields as a function of θ are determined. These are

$$N(\theta) = - T \cos \theta - (\frac{P}{2}) \text{ sgn } (\theta) \sin \theta \tag{B.2}$$

$$M(\Theta) = - T[R \cos \theta - a \cos (\theta_o)] - (\frac{P}{2})[R \text{ sgn } (\theta) \sin \quad - a \sin \theta_o], \tag{B.3}$$

in which $|\theta| < \theta_o$, T is the horizontal reaction thrust per unit length in the x-direction exerted on the panel by the pinned-end supports and

$$\text{sgn}(\theta) = \begin{cases} 1, \text{ if } \theta > 0 \\ -1, \text{ if } \theta < 0 \, . \end{cases} \tag{B.4}$$

For the deepest panel $\theta_o = \pi$. Using this specific value of θ_o, Eqs. (B.2) and (B.3) are substituted into Eq. (B.1) and integrations on θ are performed. The resulting complementary strain energy is

$$V = \frac{R\pi T^2 + (R\pi/4)P^2}{2A_{22}} + \frac{R^3\,[1 + 2(a/R)^2]T^2 + (R^3\pi/4)P^2 + (4aR^2)TP}{2D_{22}} . \tag{B.5}$$

Castigliano's second theorem states that partial derivatives of V witn respect to the forces T and P are the generalized displacements. In connection with the specific problem here, this requires

$$\frac{\partial V}{\partial P} = \Delta \qquad \text{and} \qquad \frac{\partial V}{\partial T} = 0 , \quad (B.6),(B.7)$$

where Δ is the panel displacement in the direction of the load at the point of load application. The partial derivative with respect to T (B.7) must vanish since the pinned-end supports are immovable. Eqs. (B.6) and (B.7) result in linear algebraic equations for T and P when Eq. (B.5) is used for V. If T is eliminated between them, a single equation of the form $P = K_\pi \Delta$ results, in which K_π is the global panel stiffness. After some manipulations this stiffness is

$$K = (4\pi D_{22}/R^3)[1 + 2(a/R)^2 + D_{22}/A_{22}R^2)] \cdot \{\pi^2[1 + D_{22}/(A_{22}R^2][1 + D_{22}/(A_{22}R) + 2(a/r)^2] - 16(a/R)^2\}^{-1} . \tag{B.8}$$

Specializing this for a symmetric laminate ($d = 0$, $D_{22} = \overline{D}_{22}$, etc.), and noting that the factor $D_{22}/(A_{22}R^2)$ is small with respect to unity and may be neglected for the panels in this study, the stiffness in Eq. (B.8) is adequately approximated by

$$K_\pi \simeq 12\pi\bar{D}_{22}/[a^3(3\pi^2 - 16)] \ . \tag{B.9}$$

This is the normalization constant for the ordinate in Fig. 6. It is worth stating that neglecting the factor $D_{22}/(A_{22}R^2)$ with respect to one is equivalent to neglecting the membrane portion of the complementary strain energy with respect to the bending portion; i.e. let $A_{22} \to \infty$ in Eq. (B.5).

Consider a shallow panel which is quantified by a small semi-opening angle θ_o. Statically admissible force fields for this approximation are

$$N(\theta) = - T \tag{B.10}$$

$$M(\Theta) = - (\bar{H} - R\theta^2/2)T - [sqn\ (\theta)R\ - a\theta_o](P/2) \ , \tag{B.11}$$

in which

$$\bar{H} = d + H \ . \tag{B.12}$$

The rise H (see Fig. 1) in Eq. (B.12) is closely approximated by $a\theta_o^2/2$ for a shallow panel. Substituting the functional forms of the force fields into the complementary strain energy (B.1), performing the integrations on θ, results in

$$V = (R\theta_o/D_{22}[C_T T^2 - C_{TP}TP + C_P P^2] \ , \tag{B.13}$$

in which

$$C_T = \bar{H}^2 - \bar{H}R\theta_o^2/3 + R^2\theta_o^4/20 + D_{22}/A_{22} \tag{B.14}$$

$$C_{TP} = \bar{H}a\theta_o - \bar{H}R\theta_o/2 - aR\ \theta_o^3/6 + R^2\theta_o^3/8 \tag{B.15}$$

$$C_p = (a^2\theta_o^2 + R^2\theta_o^2/3 - aR\theta_o^2)4 \ . \tag{B.16}$$

Castigliano's second theorem is applied to the complementary strain energy in Eq. (B.13), and the same procedure used to obtain the stiffness for the deepest panel described previously is followed. The resulting expression for the shallow panel stiffness is

$$K_{sh} = (D_{22}/R\theta_o)2C_T/(4C_TC_p - C_{Tp}^2) \ . \tag{B.17}$$

Finally, consider a flat panel or wide beam. The results for the shallow panel may be used to obtain the global stiffness for this case if the following limiting process is undertaken: Let $\theta_o \to 0$, such that $a\theta_o \to L/2$, where L is the beam length (see Fig. 1). In this limit, then, the coefficients in Eqs. (B.14) to (B.16) become

$$\begin{aligned} C_T &= D + D_{22}/A_{22} \ , \\ C_{Tp} &= dL/4 \ , \text{ and} \\ C_p &= L^2/48 \ . \end{aligned} \tag{B.18}$$

Substituting these limiting values into the global stiffness expression (B.17) results in a formula for the flat panel stiffness which is designated K_{bu}. After some manipulation this stiffness is

$$K_{bu} = (48D_{22}/L^3)\ (d^2 + D_{22}/A_{22})/((d/2)^2 + D_{22}/A_{22}) \ . \tag{B.19}$$

For a symmetric flat panel this becomes

$$K_b = 45\bar{D}_{22}/L^3 \ , \tag{B.20}$$

which is the normalization constant used for the ordinate in Fig. 7.